Modeling the Neural Network to Test the Basis of Working Memory in Chimpanzee

A Thesis

submitted to
Indian Institute of Science Education and Research Pune
in partial fulfillment of the requirements for the
BS-MS Dual Degree Programme

by

Suyog Sankhe

Indian Institute of Science Education and Research Pune
Dr. Homi Bhabha Road,
Pashan, Pune 411008, INDIA.

April, 2023

Supervisor: Dr. Pranay Goel

Certificate

This is to certify that this dissertation entitled Modeling the Neural Network to Test the Basis of Working Memory in Chimpanzee towards the partial fulfilment of the BS-MS dual degree programme at the Indian Institute of Science Education and Research, Pune represents study/work carried out by Suyog Sankhe at Indian Institute of Science Education and Research under the supervision of Dr. Pranay Goel, Associate Professor, Department of Biology , during the academic year 2022-2023.

Dr. Pranay Goel

Committee:

Dr. Pranay Goel

Dr. Collins Assisi

This thesis is dedicated to my mother, Rima, father, Rajendra, grandmother, Yashoda, sister, Tiksha, and brother-in-law, Aumkar, without whose love, support, and encouragement, this research could not have been possible.

Declaration

I hereby declare that the matter embodied in the report entitled Modeling the Neural Network to Test the Basis of Working Memory in Chimpanzee are the results of the work carried out by me at the Department of Biology, Indian Institute of Science Education and Research, Pune, under the supervision of Dr. Pranay Goel and the same has not been submitted elsewhere for any other degree.

Suyog Sankhe

Acknowledgments

I would like to express my deepest gratitude to my thesis advisor, Dr. Pranay Goel, for their invaluable guidance, support, and encouragement throughout my research. Their insightful feedback and constructive criticism have been instrumental in shaping the direction of my work.

I would also like to thank the member of my thesis committee, Dr. Collins Assisi, for their time, expertise, and valuable feedback that greatly contributed to the quality of my research.

ChatGPT (OpenAI, 2021) was used as an AI writing assistant for the introduction section of this thesis.

I am also grateful to my friends Mrunal, Bhavesh, Pushkar, Ritesh, Pradeep, and Darshan whose unwavering support, encouragement, and constructive criticism have helped me in numerous ways.

I would like to express my deep gratitude to my family, who have always been my source of inspiration, strength, and love. Without their support and encouragement, I would not have been able to complete this thesis.

Finally, I would like to thanks my lab members Arjun, Sandra, Somashree, Prajjwal, Sayantan, Shreya, Mukta and Rashmi for their continued support and guidance.

Abstract

Visual-spatial memory is essential for forming a representation of whatever picture the eye captures in mind. Working memory is a subset of the limited capacity part of memory that helps in cognition by integrating information modulation and transient storage (Baddeley & Hitch, 1974). The working memory makes some amount of information to be readily accessible by retention of that piece of information. A study at the Kyoto Primate Research Institute in s series of experiments showed that Ayumu, the chimpanzee they have been training for various task-based purposes, has performed better at memory-based tasks than their human counterparts (Inoue & Matsuzawa, 2007). Non-human primates are recognized for their exceptional ability to process local characteristics, whereas humans excel in integrating the local details to form a comprehensive global perception (Imura & Tomonaga, 2013). As much as visual temporal integration plays a role here, the integrated effect of attention and working memory to reproduce temporal cues is also equally important (Marchetti, 2014). Given the environment that the chimpanzees and humans live in are wildly different, the visual processing system may also have evolved some specialized structures.

In order to gain a better understanding of the complex networks within neural systems, we employ models that are capable of reconstructing network topology from various forms of data - such as neural firing data. However, it is not enough to simply rely on these models alone. It is essential that we assess their stability before generating any further data through simulation in order to obtain accurate and reliable reconstructed network parameters for analysis. Through this process, we hope to achieve greater depth and precision in our understanding of the intricate workings of these highly complex networks.

Contents

List of Figures

List of Tables

Chapter 1

Introduction

1.1 Remembering the Memory

The capacity for recollection of what the eye has seen is known as visual memory. Spatial memory records and retrieves the information as and when needed in recalling the position of an object or the occurrence of an event. Not only long-term and short-term memory but also working memory contains representations of spatial memory (WikimediaFoundation, 2022). A mechanism with a finite capacity known as working memory (WM) enables people to momentarily retain and cognize. The capacity of working memory is restricted, but it enables individuals to retain and manage data for a brief duration. It is used to complete complex tasks while keeping relevant information in mind. For example, when solving a challenging math problem, working memory is crucial in integrating information modulation and transient storage (Baddeley & Hitch, 1974). Working memory is essential for various cognitive tasks, including decision-making, problem-solving, language comprehension, and learning. In essence, working memory serves as a cognitive workspace that enables individuals to hold and manipulate information for short periods while engaged in complex tasks. The mechanism of working memory is characterized by a restricted capacity and facilitates the temporary retention and manipulation of information. This multi-faceted system encompasses various cognitive processes such as attentional control, storage capacity, and manipulation of data.(Constantinidis & Klingberg, 2016; Persuh, LaRock, & Berger, 2018).

The model put forth by Baddeley and Hitch (1974), which holds a significant standing as one of the most impactful working memory models, consists of three essential constituents: the central executive, visuospatial sketchpad, and phonological loop. The primary objective of the phonological loop is to encode and retain spoken information through two separate domains - a transitory storage unit known as the phonological store alongside an articulatory preparation process that aids individuals in preserving this data within their active memory system. On the other hand, visual and spatial information processing falls under the visuospatial sketchpad's domain with its separate sub-components a visual cache for storing visuals while the inner scribe manages the manipulation of space-based data. This model has been widely researched and expanded upon, with many studies exploring the neural and behavioral underpinnings of working memory, as well as its development and individual differences across the lifespan. Overall, working memory is a complex and dynamic cognitive system that plays a crucial role in many aspects of human cognition. Its study has significantly contributed to our understanding of how we process and manipulate information in our daily lives.

1.2 Numerals and Working Memory

The ability to remember numbers plays a crucial role in many aspects of daily life, from remembering phone numbers and addresses to performing complex mathematical calculations. The cognitive functions implicated in the registration, retention, alteration, and recovery of numerical data within the cerebral cortex are denoted as numeral information processing. This can involve the use of working memory, attention, and other cognitive processes to perform mathematical calculations, remember phone numbers, recall dates and perform other tasks that involve numerical information. The capacity and shortcomings of short-term memory and the role of attention and individual differences are important factors to consider in understanding numeral information processing. Numeral information processing is closely linked with working memory, as working memory is responsible for transiently storing and operating information, including numerical information. The phonological loop, a constituent of working memory, is paramount for processing numeric data as it permits individuals to retain and operate verbal information such as numerical figures and computations within their cognitive domain (Baddeley & Hitch, 1974). Also, attention plays an essential role in processing numerical information, and attention is crucial in the

successful encoding and retrieval of numerical information (Cowan, 2001).

1.3 Drawing Comparisions between Working Memory of Humans and Chimpanzees

Research on working memory in chimpanzees has been conducted in several studies, as these animals are known to possess advanced cognitive abilities, including the ability to use tools, understand cause and effect, and engage in complex problem-solving. Experimental results suggest that humans have a superior working memory capacity in comparison to chimpanzees. One study compared the working memory abilities of humans and chimpanzees using a delayed matching-to-sample task. The study found that humans performed significantly better than chimpanzees on this task, even when controlling for differences in perceptual and attentional abilities. The researchers concluded that this difference in working memory performance may be due to differences in the neural architecture of the prefrontal cortex, which is believed to be involved in working memory processes (Völter, Mundry, Call, & Seed, 2019; Read, Manrique, & Walker, 2022). A study by Matsuzawa et. al. in 2000 (Kawai & Matsuzawa, 2000) compared the working memory capacity of a chimpanzee and human participants on a numerical memory span task. The results showed that the chimpanzee's performance was significantly lower than that of humans, suggesting that humans have a superior working memory capacity compared to chimpanzees. Overall, these studies suggest that humans have a higher working memory capacity than chimpanzees, possibly due to differences in neural architecture and cognitive abilities. While research generally suggests that humans have a superior working memory capacity compared to chimpanzees, there are some specific domains in which chimpanzees may have superior working memory abilities.

One of the most groundbreaking studies on this subject was steered by Matsuzawa and colleagues in 2007 (Inoue & Matsuzawa, 2007), which shed light on the remarkable extent of chimpanzee working memory capacity and processing speed. In this study, five chimpanzees were trained to memorize the location and order of numerals on a touch screen monitor. The numerals appeared on the screen for a fraction of a second, after which they were replaced by white squares in their previous locations. The chimpanzees were then

required to touch the squares in ascending numerical order, demonstrating their memory of the numeral positions and sequence. The results of this study were astonishing, as the chimpanzees not only demonstrated a remarkable ability to recall the positions and sequence of numerals but also exhibited faster processing speed than humans on this task. The findings of this study challenge the conventional belief that humans possess superior working memory capacities in comparison to other primates. These findings suggest that chimpanzees possess advanced cognitive abilities that were previously attributed solely to humans and highlight the need for further research on animal cognition. Moreover, the results of this experimental study have significant consequences for our understanding of cognitive evolution. They can serve as a foundation for future research aimed at uncovering the underlying neural mechanisms that contribute to the enhancement of such advanced cognitive abilities in both humans and non-human primates.

1.3.1 Why Use Chimpanzees for Working Memory Studies?

Chimpanzees are often selected for working memory studies because they are one of our closest living relatives and share many cognitive and behavioral similarities with humans. In fact, chimpanzees are one of the few non-human primates that have been shown to perform well on a range of cognitive tasks, including those related to working memory. Studies have found that chimpanzees exhibit impressive working memory capabilities, such as the ability to remember the location and identity of hidden food items or to remember the order of events in a sequence (Cantwell, Buckholtz, Atencia, & Rosati, 2022). Moreover, chimpanzees are highly intelligent and have been observed to use complex problem-solving strategies in the wild, such as using tools to obtain food or communicating with each other through a variety of vocalizations and gestures. This suggests that they have advanced cognitive abilities that may be comparable to those of humans in some respects. Studying chimpanzee working memory can provide insight into the cognitive and neural mechanisms that underlie working memory in humans, as well as shed light on the evolution of cognitive abilities across different species. Additionally, because chimpanzees have complex social lives, studying their working memory can provide insight into the cognitive processes underlying their social behavior and decision-making. Overall, chimpanzees are an ideal species for studying working memory because they have many cognitive and behavioral similarities to humans and have been shown to perform well on a range of

cognitive tasks.

1.4 Working Models of Working Memory

1.4.1 In Humans

According to neuronal oscillator models, the synchronization of neural oscillators is responsible for maintaining continual neural activity and sustaining working memory. These models propose that only a small subset of neurons are responsible for sustained firing during this process, which occurs due to their synchronized oscillatory behavior. This synchronization is thought to occur through recurrent synaptic connections between neurons in a local neural network, such as the prefrontal cortex (Singer, 2009; Loebel & Tsodyks, 2002). These connections facilitate the continuous exchange of information, allowing for the maintenance and manipulation of stored information in working memory (Lodi, Rossa, Sorrentino, & Storace, 2020). Furthermore, this process is thought to be highly dynamic and flexible, adapting to changing cognitive demands and environmental inputs. Summarized below are few models that underline this theory.

1.4.1.1 The Prefrontal Cortex Model

The Prefrontal Cortex Model: This model proposes that a network of prefrontal neurons supports working memory through continued activity during the task's delay period. This continual activity can be maintained through recurrent excitatory connections among the neurons, which are modulated by inhibitory feedback (Compte, 2000).

1.4.1.2 The Synaptic Scaling Model

This model proposes that working memory is mediated by synaptic scaling, which is the process by which the strength of synapses is modulated to maintain a stable level of network activity. The model suggests that synaptic scaling can be regulated by neuromodula-

tors such as dopamine, which can modulate the strength of synaptic connections based on the reward value of the information being held in working memory (Lisman & Otmakhova, 2001).

1.4.1.3 The Theta-Gamma Network Model

This model suggests that working memory involves the coupling of theta and gamma oscillations in different brain regions. Theta oscillations are slower and reflect the synchronization of neuronal firing across large populations, while gamma oscillations are faster and reflect the synchronization of neuronal firing within smaller populations. The model proposes that theta oscillations provide a temporal framework for the activation and maintenance of working memory representations, while gamma oscillations provide the detailed content of those representations (Lisman & Jensen, 2013).

1.4.2 In Chimpanzees

There is limited research on coupled oscillator network models for working memory in chimpanzees. However, some studies have investigated neural oscillations in the prefrontal cortex of chimpanzees during working memory tasks, which could be related to these types of models. Additionally, these studies have provided valuable insights into the underlying neural mechanisms and their potential similarities with human working memory processes. However, more research is needed to investigate the precise neural mechanisms underlying working memory in chimpanzees and how they relate to these models. We use these studies as a foundation for developing coupled oscillator network models for working memory in chimpanzees. In this thesis, we apply algorithms, such as the Kuramoto model and the phase response curve (PRC) method, which helps infer the model and network topology from a given dataset in a system, to simulate coupled oscillator networks in the chimpanzee prefrontal cortex during working memory tasks (Panaggio, Ciocanel, Lazarus, Topaz, & Xu, 2019).

Chapter 2

Preliminaries

2.1 The Kuramoto Model

The Kuramoto model, created by Japanese physicist Yoshiki Kuramoto in 1975 (Kuramoto, 2005), is a mathematical representation utilized to explain the synchronization of interconnected oscillators.

It comprises N individual oscillators with distinctive natural frequencies that connect through a coupling term relying on their phase disparity. The oscillator's phases progress over time according to both their inherent frequency and the impact of other surrounding oscillators.

The equation for the Kuramoto model can be represented as follows:

$$\frac{d\theta_i}{dt} = \omega_i + \frac{K}{N}\sum_{j=1}^{N} \sin(\theta_j - \theta_i) \tag{2.1}$$

The given equation denotes the phase θ_i of each oscillator, its respective natural frequency ω_i, and the total number of oscillators N. The coupling strength is represented by K, while interaction between oscillators is expressed through a summation over j, and their phase difference via $\sin(\theta_j - \theta_i)$.

This equation signifies that the inherent frequency of an oscillator, as well as its in-

teractions with other oscillators through coupling terms, determine changes in its phase. When these coupling strengths are strong enough to synchronize phases among different oscillators, collective behavior emerges. The Kuramoto model has been widely studied in physics, mathematics, and other fields, and has applications in areas such as neuroscience, power grid stability, and chemical reactions. It is often used to investigate emergent phenomena, such as the spontaneous synchronization of fireflies or the coordinated behavior of cells in the heart.

2.2 The Phase response curve (PRC)

The phase response curve (PRC) is a tool applied to study the response of oscillators to external perturbations, such as stimuli or inputs. It describes how the phase of an oscillator is shifted by a small perturbation at different points in its oscillatory cycle.

The phase response curve (PRC) is commonly depicted in a graphical form as a curve that illustrates the alteration of phase brought about by an insignificant disturbance concerning the oscillator's initial stage. The normalization of PRC is generally done to ensure that the overall area covered under it equals one.

The phase response curve (PRC) can be represented mathematically as a function that describes how the phase of an oscillator changes in response to a perturbation. The PRC, represented as $\Delta\phi(\theta)$ with θ indicating the oscillator's phase during perturbation, is capable of expressing alterations in phase resulting from such disturbance. The duration of perturbation can be depicted by Δt, while the corresponding change in phase may be expressed as $\Delta\phi = \Delta\phi(\theta) \times \Delta t$.

The PRC is an important tool for studying the dynamics of oscillators and understanding how they respond to perturbations. It has applications in fields such as neuroscience, physiology, and engineering.

2.3 Coupled neural networks

Coupled neural networks refer to a collection of neural networks that interact with each other through a set of connections or couplings. The networks can be either identical or heterogeneous and can interact in various ways, including through mutual feedback, feedforward connections, or lateral connections.

Coupled neural networks can be analyzed using various mathematical tools, such as graph theory, dynamical systems theory, and statistical physics. These tools can be used to understand the behavior of the networks, predict their dynamics, and optimize their performance.

2.4 Adjacency matrix

In the field of graph theory, a square matrix known as an adjacency matrix is utilized to depict a given graph. The vertices of the graph are represented by the rows and columns in the matrix while each entry indicates whether there exists an edge between two vertices. Notably, for a graph G comprising n vertices, its corresponding adjacency matrix can be denoted as $A(G)$ and takes up dimensions of $n \times n$. In particular, if vertex i connects with vertex j, then their respective entry $(a_{ij}) = 1$, otherwise it equals 0. Moreover, if said graph lacks directionality (undirected), then all entries have symmetry such that $(a_{ij}) = (a_{ji})$ holds true for any pair (i, j). An alternative representation method involves using this notation:

$$A(G) = \begin{bmatrix} a_{11} & a_{12} & a_{13} & \cdots & a_{1n} & a_{21} & a_{22} & a_{23} & \cdots & a_{2n} & \vdots & \vdots \\ \ddots & \vdots & a_{n1} & a_{n2} & \cdots & a_{nn} & & & & & & \end{bmatrix} \tag{2.2}$$

In the matrix, a_{ij} denotes the value located in row i and column j.

2.5 The Van der Pol Equation

The Van der Pol oscillator, which exhibits nonlinear behavior and damping, is frequently employed as a theoretical framework for numerous physical systems such as electrical circuits and biological organisms. The system's dynamics are summarized in the second-order differential equation given below:

$$\frac{d^2x}{dt^2} - \mu(1 - x^2)\frac{dx}{dt} + x = 0 \tag{2.3}$$

where the position of the oscillator is x, μ is a parameter that controls the strength of the damping and the non-linearity, and t is time.

2.6 Spike train model

A spike train model is a mathematical model that is used to describe the pattern of electrical impulses (spikes) that are generated by neurons in the brain. Neurons communicate with each other through these spikes, and the pattern of spikes has been shown to be important for a variety of brain functions, including perception, cognition, and behavior.

Spike train models commonly delineate the likelihood of a neuron discharging an action potential (spike) at a specified moment, conditional upon the stimuli received from sensory inputs or other neurons. These models can be either deterministic or stochastic, depending on the level of randomness that is included in the model.

Chapter 3

The Prequel

Assuming we have the time-series data of the neuronal firing; we employ the method given in the study done by Panaggio et al., 2019 (Panaggio et al., 2019), which involves using a mathematical model known as the Kuramoto model to analyze and predict the synchronization behavior of coupled oscillators.The methodology of the paper comprises the generation of time-series data for oscillator phases followed by the calculation of their respective phase velocities. Prior to model reconstruction, a nonlinear differential equation set is applied in order to formulate an optimization problem which aims at minimizing mean squared error associated with estimated phase velocities. By using numerical minimization techniques, values for ideal parameters such as the adjacency matrix of network connections, intensity of oscillator coupling and frequencies can be obtained.

The estimated parameters are then used to rebuild the model, which is validated by comparing the simulated and experimental phase velocities. The Kuramoto model has been found to be highly effective in predicting the synchronization behavior of neuronal firing and can provide valuable insights into the underlying mechanisms (Guo, Zhang, Li, Wang, & Yu, 2021).

This method builds on the recipe given by Shandilya & Timme, 2011 (Shandilya & Timme, 2011), which offers the theory of direct reconstruction from dynamical trajectories. The methodology can be divided into the following steps:

1. **Define the model:** The first step is to define the model of the coupled oscillator net-

work. The dynamics of the oscillator is defined by differential equations that describe the dynamics of each oscillator in the network and the interactions between them.

2. **Simulate the model:** The next step is to simulate the model to generate synthetic data. This is done by solving the differential equations numerically using an integration method, for example the Runge-Kutta method of the fourth order. The simulation generates time-series data for each oscillator in the network.

3. **Estimation of the derivatives:** The derivatives are estimated using a first-order approximation and a matrix equation is set up using the phases and the estimated derivatives.

4. **Identify the network structure:** The correlation matrix is used to identify the network structure of the coupled oscillator network. The network structure is represented as an adjacency matrix, which indicates which oscillators are connected to each other. The adjacency matrix is estimated using a thresholding method that sets a threshold on the absolute value of the correlation coefficients.

5. **Estimate the coupling functions:** Once the network structure is identified, the next step is to estimate the coupling functions that describe the interactions between the oscillators.

3.1 Equations for the dynamics of the oscillator

$$\frac{d}{dt}x_i = f_i(x_i) + \sum_{j=1}^{N} J_{ij} g_{ij}(x_i, x_j), \tag{3.1}$$

Taking the simple case with two unit osicillators x_1 and x_2, we obtain
M equations of the form,

$$\dot{x_1} = f_1(x_1) + J_{11}g_{11}(x_1, x_1) + J_{12}g_{12}(x_1, x_2) \tag{3.2}$$

$$\dot{x_2} = f_2(x_2) + J_{21}g_{21}(x_2, x_1) + J_{22}g_{22}(x_2, x_2) \tag{3.3}$$

$$\dot{x_1} - f_1(x_1) = J_{11}g_{11}(x_1, x_1) + J_{12}g_{12}(x_1, x_2) \tag{3.4}$$

$$\dot{x_2} - f_2(x_2) = J_{21}g_{21}(x_2, x_1) + J_{22}g_{22}(x_2, x_2) \tag{3.5}$$

$$\tag{3.6}$$

Putting $\dot{x_1} - f_1(x_1) = X_1$ & $\dot{x_2} - f_2(x_2) = X_2$,

$$X_1 = J_{11}g_{11}(x_1, x_1) + J_{12}g_{12}(x_1, x_2) \tag{3.7}$$

$$X_2 = J_{21}g_{21}(x_2, x_1) + J_{22}g_{22}(x_2, x_2) \tag{3.8}$$

$$X_i = J_i G_i \tag{3.9}$$

$$\tag{3.10}$$

3.2 Reconstruction of network topology from dynamical trajectories

$$E_i(\hat{J_i}) = \frac{1}{N * M} \sum_{m=1}^{M} (x_{im} - \sum_{k=1}^{N} \hat{J_{ik}} g_{ikm})^2 \tag{3.11}$$

For N = 2 and M = 2 (2-unit oscillator and 3 time-points)

$$E_i(\hat{J_i}) = \frac{1}{6} \sum_{m=1}^{3} (x_{im} - \sum_{k=1}^{2} \hat{J_{ik}} g_{ikm})^2 \tag{3.12}$$

We have the dynamics,

$$\begin{bmatrix} X_{1,1} & X_{1,2} & X1,3 \end{bmatrix}_{1\times 3} = \begin{bmatrix} J_{11} & J_{12} \end{bmatrix}_{1\times 2} \begin{bmatrix} g_{11,1} & g_{11,2} & g_{11,3} \\ g_{12,1} & g_{12,2} & g_{12,3} \end{bmatrix}_{2\times 3} \tag{3.13}$$

Which writing in the form of eq. (3.12) gives,

$$E_1(\hat{J}_1) = (X_{1,1} - J_1 g_{1,1})^2 + (X_{1,2} - J_1 g_{1,2})^2 + (X_{1,3} - J_1 g_{1,3})^2 \tag{3.14}$$

Differentiating eq. (3.14) w.r.t. $\hat{J_{ik}}$

$$\begin{aligned}\frac{\partial E_1(\hat{J}_1)}{\partial(J_{11})} &= 2(X_{1,1} - J_{11}g_{11,1} - J_{12}g_{12,1})(-g_{11,1}) \\ &+ 2(X_{1,2} - J_{11}g_{11,2} - J_{12}g_{12,2})(-g_{11,2}) \\ &+ 2(X_{1,3} - J_{11}g_{11,3} - J_{12}g_{12,3})(-g_{11,3})\end{aligned}$$

Equating $\frac{\partial E_1(\hat{J}_1)}{\partial\ (J_{11})} \stackrel{!}{=} 0$ we get

$$\begin{aligned}X_{1,1}g_{11,1} + X_{1,2}g_{11,2} + X1,3g_{11,3} &= J_{11}(g_{11,1}^2 + g_{11,2}^2 + g_{11,3}^2) \\ &+ J_{12}(g_{11,1}g_{12,1} + g_{11,2}g_{12,2} + g_{11,3}g_{12,3})\end{aligned}$$

$$\begin{aligned}X_{1,1}g_{12,1} + X_{1,2}g_{12,2} + X1,3g_{12,3} &= J_{11}(g_{11,1}g_{12,1} + g_{11,2}g_{12,2} + g_{11,3}g_{12,3}) \\ &+ J_{12}(g_{12,1}^2 + g_{12,2}^2 + g_{12,3}^2)\end{aligned}$$

$$\begin{bmatrix}X_{1,1} & X_{1,2} & X1,3\end{bmatrix}_{1\times 3}\begin{bmatrix}g_{11,1} & g_{12,1} \\ g_{11,2} & g_{12,2} \\ g_{11,3} & g_{12,3}\end{bmatrix}_{3\times 2} = \begin{bmatrix}J_{11} & J_{12}\end{bmatrix}_{1\times 2}\begin{bmatrix}g_{11,1}^+ g_{11,2}^2 + g_{11,3}^2 & x \\ x & g_{11,1}^+ g_{11,2}^2 + g_{11,3}^2\end{bmatrix}_{2\times 3}$$

where $x = g_{11,1}g_{12,1} + g_{11,2}g_{12,2} + g_{11,3}g_{12,3}$

$$J_1 = X_1 G_1^T (G_1 G_1^T)^{-1} \tag{3.15}$$

3.3 Minimization generalization for the reconstructed network parameter

$$\hat{J}_i = X_i G_i^T (G_i G_i^T)^{-1} \tag{3.16}$$

$$\hat{J}_1 = X_1 \begin{bmatrix} f_{12_1} \\ f_{12_2} \\ f_{12_3} \end{bmatrix}_{3\times 1} \left(\begin{bmatrix} f_{12_1} & f_{12_2} & f_{12_3} \end{bmatrix}_{1\times 3} \begin{bmatrix} f_{12_1} \\ f_{12_2} \\ f_{12_3} \end{bmatrix}_{3\times 1} \right)^{-1} \tag{3.17}$$

$$\hat{J}_1 = X_1 \begin{bmatrix} f_{12_1} \\ f_{12_2} \\ f_{12_3} \end{bmatrix}_{3\times 1} \left(\begin{bmatrix} (f_{12_1}^2 + f_{12_2}^2 + f_{12_3}^2 \end{bmatrix}_{1\times 1} \right)^{-1} \tag{3.18}$$

$$\tag{3.19}$$

Taking $(f_{12_1}^2 + f_{12_2}^2 + f_{12_3}^2)$ as a,

$$\hat{J}_1 = \begin{bmatrix} X_{1_1} & X_{1_2} & X_{1_3} \end{bmatrix}_{1\times 3} \begin{bmatrix} f_{12_1} \\ f_{12_2} \\ f_{12_3} \end{bmatrix}_{3\times 1} \begin{bmatrix} (\frac{1}{a}) \end{bmatrix}_{1\times 1} \tag{3.20}$$

$$\hat{J}_1 = \begin{bmatrix} X_{1_1} & X_{1_2} & X_{1_3} \end{bmatrix}_{1\times 3} \begin{bmatrix} \frac{f_{12_1}}{a} \\ \frac{f_{12_2}}{a} \\ \frac{f_{12_3}}{a} \end{bmatrix}_{3\times 1} \tag{3.21}$$

$$\hat{J}_1 = \left[\left((\frac{X_{1_1} f_{12_1}}{a}) + (\frac{X_{1_2} f_{12_2}}{a}) + (\frac{X_{1_3} f_{12_3}}{a}) \right) \right] \tag{3.22}$$

3.4 Deriving the equations for Van der Pol oscillators

Rewriting eq. (3.11) explicitly for J_i:

$$E_i(\hat{J}_i) = \frac{1}{N * M} \sum_{m=1}^{M} (x_{im} - \sum_{k=1}^{N} \hat{J}_{ik} g_{ikm})^2 \tag{3.23}$$

$$\hat{J}_i = X_i G_i^T (G_i G_i^T)^{-1} \tag{3.24}$$

The Van der Pol equation:

$$\dot{x} = u(x - \frac{1}{3}x^3 - y) \tag{3.25}$$

$$\dot{y} = \frac{1}{u}x \tag{3.26}$$

(3.27)

Coupling the Van der Pol equations through the x term and writing for 2 unit oscillators:

$$\dot{x_1} = u_1(x_1 - \frac{1}{3}x_1^3 - y_1) + a_{12}(x_1 - x_2) + a_{11}(x_1 - x_1) \tag{3.28}$$

$$\dot{y_1} = \frac{1}{u_1}x_1 \tag{3.29}$$

$$\dot{x_2} = u_2(x_2 - \frac{1}{3}x_2^3 - y_2) + a_{21}(x_2 - x_1) + a_{22}(x_2 - x_2) \tag{3.30}$$

$$\dot{y_2} = \frac{1}{u_2}x_2 \tag{3.31}$$

$$X_1 = \dot{x_1} - u_1(x_1 - \frac{1}{3}x_1^3 - y_1) \text{ \&} \tag{3.32}$$

$$X_2 = \dot{x_2} - u_2(x_2 - \frac{1}{3}x_2^3 - y_2) \text{ gives} \tag{3.33}$$

$$X_1 = a_{12}(x_1 - x_2) \text{ \&} \tag{3.34}$$

$$X_2 = a_{21}(x_2 - x_1) \tag{3.35}$$

(3.36)

Deriving the minimization solution for Van der Pol equation for 1^{st} unit with m = 5:

$$\hat{J}_i = X_i G_i^T (G_i G_i^T)^{-1} \tag{3.37}$$

$$\hat{J}_1 = X_1 \begin{bmatrix} f_{12_1} \\ f_{12_2} \\ f_{12_3} \\ f_{12_4} \\ f_{12_5} \end{bmatrix}_{5x1} \left(\begin{bmatrix} f_{12_1} & f_{12_2} & f_{12_3} & f_{12_4} & f_{12_5} \end{bmatrix}_{1x5} \begin{bmatrix} f_{12_1} \\ f_{12_2} \\ f_{12_3} \\ f_{12_4} \\ f_{12_5} \end{bmatrix}_{5x1} \right)^{-1} \tag{3.38}$$

$$\hat{J}_1 = X_1 \begin{bmatrix} f_{12_1} \\ f_{12_2} \\ f_{12_3} \\ f_{12_4} \\ f_{12_5} \end{bmatrix}_{5x1} \left(\left[(f_{12_1}^2 + f_{12_2}^2 + f_{12_3}^2 + f_{12_4}^2 + f_{12_5}^2) \right]_{1x1} \right)^{-1} \tag{3.39}$$

(3.40)

Taking $(f_{12_1}^2 + f_{12_2}^2 + f_{12_3}^2 + f_{12_4}^2 + f_{12_5}^2)$ as a,

$$\hat{J}_1 = \begin{bmatrix} X_{1_1} & X_{1_2} & X_{1_3} & X_{1_4} & X_{1_5} \end{bmatrix}_{1x5} \begin{bmatrix} f_{12_1} \\ f_{12_2} \\ f_{12_3} \\ f_{12_4} \\ f_{12_5} \end{bmatrix}_{5x1} \left[(\tfrac{1}{a}) \right]_{1x1} \tag{3.41}$$

$$\hat{J}_1 = \begin{bmatrix} X_{1_1} & X_{1_2} & X_{1_3} & X_{1_4} & X_{1_5} \end{bmatrix}_{1x5} \begin{bmatrix} \frac{f_{12_1}}{a} \\ \frac{f_{12_2}}{a} \\ \frac{f_{12_3}}{a} \\ \frac{f_{12_4}}{a} \\ \frac{f_{12_5}}{a} \end{bmatrix}_{5x1} \tag{3.42}$$

$$\hat{J}_1 = \left[\left((\tfrac{X_{1_1} f_{12_1}}{a}) + (\tfrac{X_{1_2} f_{12_2}}{a}) + (\tfrac{X_{1_3} f_{12_3}}{a}) + (\tfrac{X_{1_4} f_{12_4}}{a}) + (\tfrac{X_{1_5} f_{12_5}}{a}) \right) \right] \tag{3.43}$$

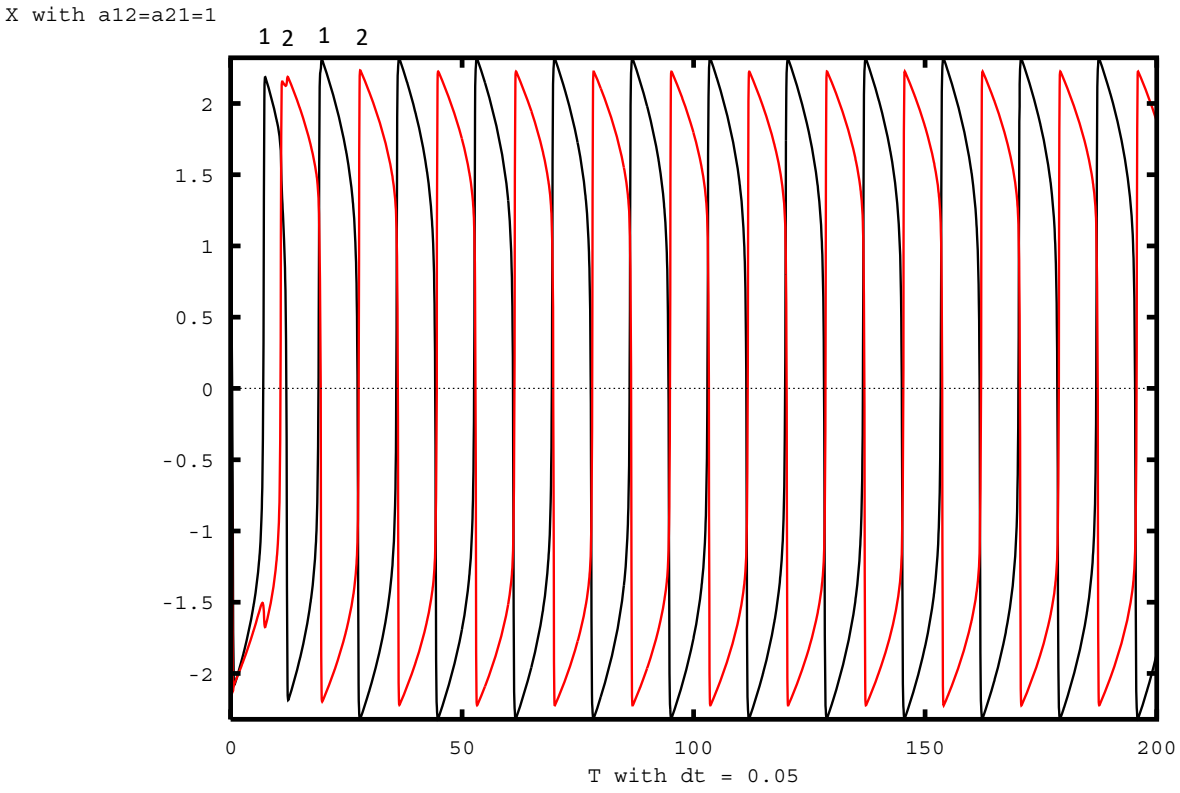

Figure 3.1: Phase time plot for coupled Van der Pol equation with 2-unit oscillators. Black Line represents unit 1 and red line represents unit 2. The oscillators are shown to be out of phase w.r.t each other. Both units are initialized with an initial phase equal to 1 and differentiation time of 0.05.

3.5 Kuramoto model as the backbone and Van der Pol equations for oscillator dynamics

We use different sets of input coupling strengths and different dt's to test the quality of reconstruction and compare the input strengths to the reconstructed ones like the plot shown in fig. 3.1. The sets of input and reconstructed coupling strengths are provided in table 3.1.

dt	Time interval	Input Coupling Strengths		Reconstructed Coupling Strengths	
		J1	J2	J1	J2
0.0005	200	1	1	1.0001	1.0001
0.05	200	1	1	1.0073	1.0076
0.15	200	1	1	-2.1784	-2.1908
0.15	200 (II)	1	1	1.0237	1.0222
0.05	40	1	1	1.0085	1.0084
0.15	40(II)	1	1	1.0262	1.0228
0.05	200	3	2	3.0098	2.0074
0.005	200	4	8	4.0009	8.0016
0.05	200	4	8	4.6251	4.3352
0.005	200	8	4	8.0014	4.0010
0.05	200	8	4	5.2843	4.5798

Table 3.1: Comparision between input (true) and reconstructed coupling strengths given by J's. Here (*) refers to the integrator method vode while all others are with the Runge-Kutta method.

From the reconstructed values of the coupling strengths, we can see that the values are successfully recovered when the dt is small enough that the information is not lost, and the reconstructions are not accurate if the dt is small, which is obvious enough. So, while we do have a method of reconstructing the coupling strength, it was observed that when the system complexity increases, i.e., the number of unit oscillators increase, the reconstruction almost always fails and does not give the correct coupling strengths. This limitation may be attributed to the high dimensionality of the system and the difficulty in accurately capturing all interactions among unit oscillators. Therefore, this method may be suitable for smaller and less complex systems, but alternative approaches may be necessary for larger or more intricate systems.

Chapter 4

Models, Methodology, and Derivations

4.1 Spike-train model

Another model we use for reconstruction in this thesis is the spike-train reconstruction model by Cestnik et. al., 2017 (Cestnik & Rosenblum, 2017). The underlying premise of this model is that it is possible to reconstitute a neuron's spiking behavior through its presynaptic inputs. Following is the methodology that will be used in the thesis with certain modifications from the paper.

1. **Model and simulation:** The first step is to define the model and simulation. Using a pulse-coupled oscillator model, which consists of a set of oscillators that are coupled together via pulses. The dynamics of each oscillator are governed by a phase variable, and the coupling between oscillators is modeled as a pulse that advances the phase of the receiving oscillator by a fixed amount.

2. **Data generation:** Simulation is used to generate spike train data from the network. A threshold for the phase variable is defined, such that when an oscillator's phase crosses the threshold, a spike is generated. Spike train data is generated by simulating the network dynamics for a period of time and recording the times at which spikes occur.

3. **Network inference and analysis:** We start with an initial guess for the connectivity

matrix, which is a binary matrix indicating which oscillators are connected to each other. A comparison between the inferred network and the ground truth network is done, which is the true connectivity matrix used to generate the spike train data.

We now go through how we build the model and define the equations that follow. The

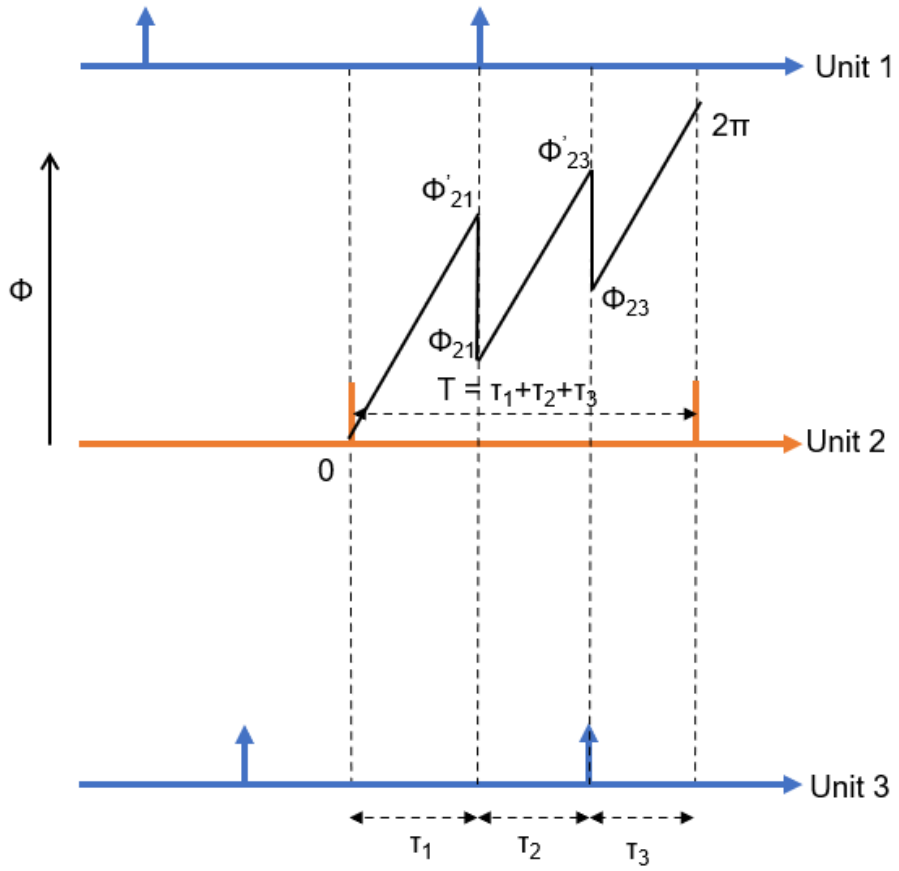

Figure 4.1: Illustration of phase-time plot of oscillator 2 in the 3-unit oscillator

neurons are limit cycle oscillators which go form 0 to 2π. The spiking of an unit affects other unit as a function of the coupling strength between the two units and the phase response curve (PRC) of the same unit that is being impacted. The inter-spike intervals

are given by $\tau's$

$$\phi_{21}^{'} = \omega_2 \tau_1 \tag{4.1}$$
$$\phi_{21} = \phi_{21}^{'} + \varepsilon_{21} \sin(\phi_{21}^{'}) \tag{4.2}$$
$$\phi_{23}^{'} = \omega_2(\tau_1 + \tau_2) + \varepsilon_{23} \sin(\phi_{23}^{'}) \tag{4.3}$$
$$\phi_{23} = \phi_{23}^{'} + \varepsilon_{23} \sin(\phi_{23}^{'}) \tag{4.4}$$
$$2\pi = \omega_2 T + \varepsilon_{21} \sin(\phi_{21}^{'}) + \varepsilon_{23} \sin(\phi_{23}^{'}) \tag{4.5}$$

4.2 Spike-train equations for 3-unit oscillator

Equations for the firing pattern 1-2-3 as shown in fig. 4.2:

For the third oscillator,

$$\phi_3 = \omega_3 \tau_1 \tag{4.6}$$
$$2\pi = \omega_3 T - \varepsilon_{32} \sin(\phi_3) \tag{4.7}$$
$$2\pi = \omega_3 T - \varepsilon_{32} \sin(\omega_3 \tau_1) \tag{4.8}$$

For the second oscillator,

$$\phi_{21} = \omega_2 \tau_2 \tag{4.9}$$
$$\phi_{23} = \omega_2(\tau_2 + \tau_3) - \varepsilon_{21} \sin(\omega_2 \tau_2) \tag{4.10}$$
$$2\pi = \omega_2 T - \varepsilon_{21} \sin(\omega_2 \tau_2) - \varepsilon_{23} \sin(\omega_2(\tau_2 + \tau_3) - \varepsilon_{21} \sin(\omega_2 \tau_2)) \tag{4.11}$$

For the first oscillator,

$$\phi_1 = \omega_1(\tau_3 + \tau_1) \tag{4.12}$$
$$2\pi = \omega_1 T - \varepsilon_{12} \sin(\omega_1(\tau_3 + \tau_1)) \tag{4.13}$$

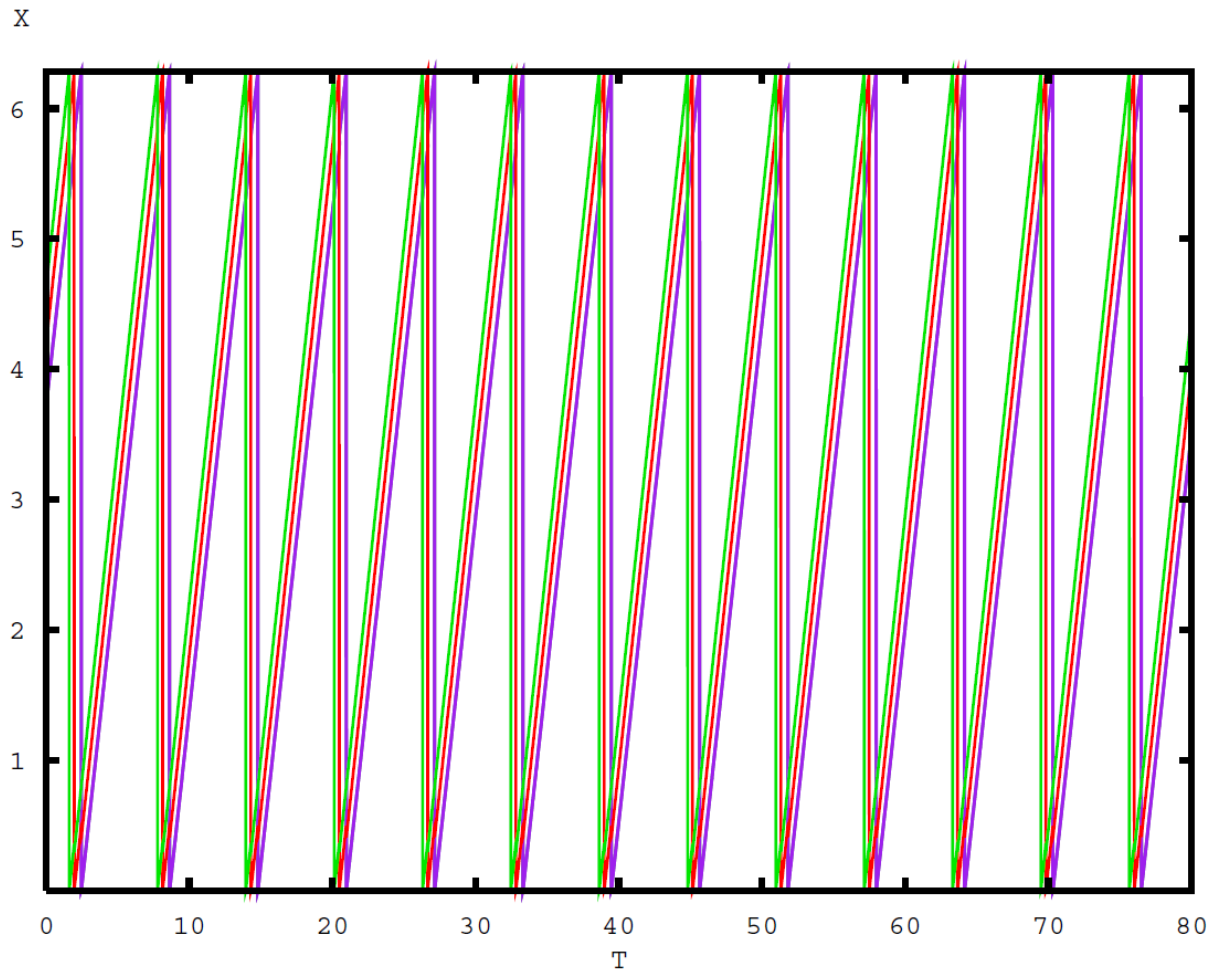

Figure 4.2: Plot of phases of 3-unit oscillators 1,2, and 3 shown in green, red and purple lines respectively as a function of time

4.3 Re-deriving the spike-train equations for 3-unit oscillator

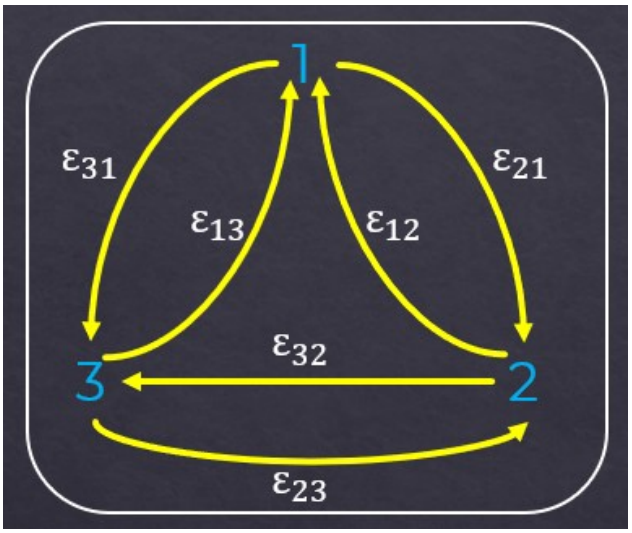

Figure 4.3: All-to-all globally coupled 3-unit oscillator

The network topology for the globally-coupled network and the phase-time plot for the 3-unit oscillator is shown in fig. 4.3 and fig. 4.4 respectively.

For the second oscillator and the firing pattern 1-3-2, considering $\omega_1 = \omega_2 = \omega_3 = \omega, \tau_1 = \tau_2 = \tau_3 = \tau = T/3$ & $\varepsilon_{ij} = \varepsilon$

$$\phi_{21}^{'} = \omega\tau \tag{4.14}$$
$$\phi_{21} = \phi_{21}^{'} + \varepsilon \sin(\phi_{21}^{'}) \tag{4.15}$$
$$\phi_{23}^{'} = \omega(\tau + \tau) + \varepsilon \sin(\phi_{21}^{'}) \tag{4.16}$$
$$\phi_{23} = \phi_{23}^{'} + \varepsilon \sin(\phi_{31}^{'}) \tag{4.17}$$
$$2\pi = \omega T + \varepsilon \sin(\phi_{21}^{'}) + \varepsilon \sin(\phi_{31}^{'}) \tag{4.18}$$

Here, the $\phi^{'}$'s are the phases before the phase transition occurs

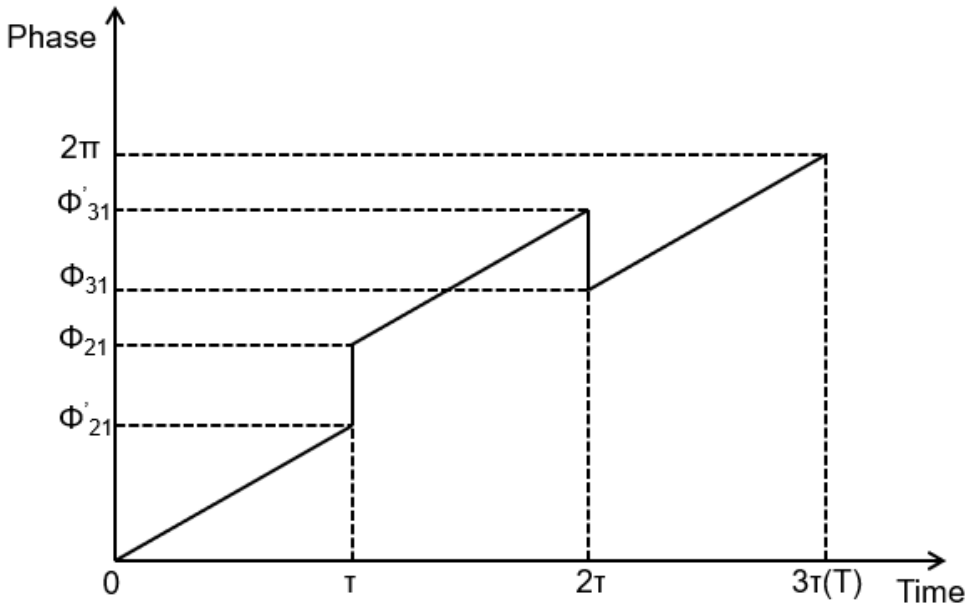

Figure 4.4: Illustration of phase-time plot of oscillator 2 in the 3-unit oscillator for the firing pattern 1-3-2 for 3-unit oscillator

4.4 Spike-train equations for 4-unit oscillators

The network topology for the all-to-all coupled 4-unit oscillator is given in fig. 4.5.

For the second oscillator and the firing pattern 1-3-2-4, considering $\omega_1 = \omega_2 = \omega_3 = \omega_4 = \omega, \tau_1 = \tau_2 = \tau_3 = \tau_4 = \tau = T/4$ & $\varepsilon_{ij} = \varepsilon$

$$\phi'_{24} = \omega\tau \tag{4.19}$$

$$\phi'_{21} = 2\omega\tau + \varepsilon_1 \sin(\phi'_{24}) \tag{4.20}$$

$$\phi'_{23} = 3\omega\tau + \varepsilon_1 \sin(\phi'_{24}) + \varepsilon_2 \sin(\phi'_{21}) \tag{4.21}$$

$$2\pi = \omega T + \varepsilon_1 \sin(\phi'_{24}) + \varepsilon_2 \sin(\phi'_{21}) + \varepsilon_3 \sin(\phi'_{23}) \tag{4.22}$$

4.5 Spike-train equations for 5-unit oscillators

The network topology for the all-to-all coupled 4-unit oscillator is given in fig. 4.6.

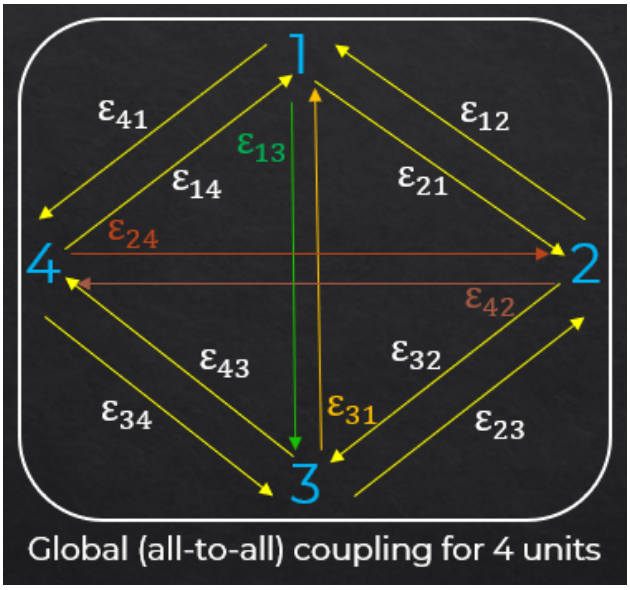

Figure 4.5: All-to-all globally coupled 4-unit oscillator

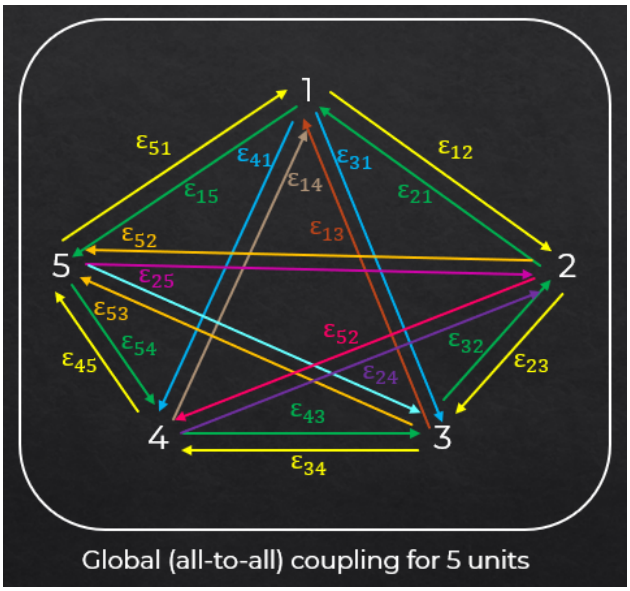

Figure 4.6: All-to-all globally coupled 5-unit oscillator

For the second oscillator and the firing pattern 1-3-2-4-5, considering $\omega_1 = \omega_2 = \omega_3 = \omega_4 = \omega_5 = \omega, \tau_1 = \tau_2 = \tau_3 = \tau_4 = \tau_5 = \tau = T/4$ & $\varepsilon_{ij} = \varepsilon$

$$\phi_{24}^{'} = \omega\tau \tag{4.23}$$

$$\phi_{25}^{'} = 2\omega\tau + \varepsilon \sin(\phi_{24}^{'}) \tag{4.24}$$

$$\phi_{21}^{'} = 3\omega\tau + \varepsilon \sin(\phi_{24}^{'}) + \varepsilon \sin(\phi_{25}^{'}) \tag{4.25}$$

$$\phi_{23}^{'} = 3\omega\tau + \varepsilon \sin(\phi_{24}^{'}) + \varepsilon \sin(\phi_{25}^{'}) + \varepsilon \sin(\phi_{21}^{'}) \tag{4.26}$$

$$2\pi = \omega T + \varepsilon \sin(\phi_{24}^{'}) + \varepsilon \sin(\phi_{25}^{'}) + \varepsilon \sin(\phi_{21}^{'}) + \varepsilon \sin(\phi_{23}^{'}) \tag{4.27}$$

4.6 Data Simulation and Generation

The data was generated by simulation using XPP-Aut software. XPP-Aut is a computational tool for modeling and simulating dynamical systems. We write the differential equations in the form of 'ode' file (.ode) and then generate the time-series data for a coupled oscillator with different parameter values and initiation conditions. This approach allows for the systematic exploration of the parameter space and provides a large dataset for analysis.

Chapter 5

Data Analysis

5.1 Spike-train model data

We use the methods and equations given in the paper (Cestnik & Rosenblum, 2017) to develop the set of equations and data simulation that follows. Figure 5.1 represents the firing pattern and the time-spacing between the peaks of the 3 oscillators for the 3-unit oscillator case.

5.1.1 3-unit oscillator case

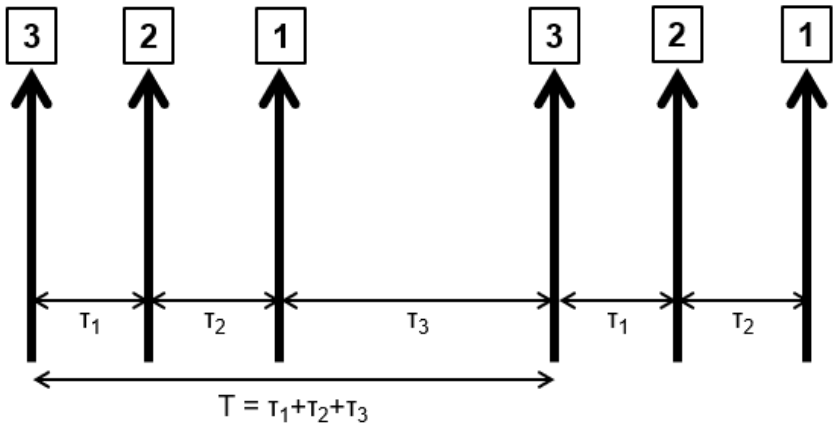

Figure 5.1: Illustration of the 3-unit oscillators 1,2, and 3 and the difference between them shown by the tau's, T represents one complete cycle of an oscillator

Given (from XPP), $\omega_1 = 1, \omega_2 = 1.02, \omega_3 = 1.03, T = 6.17, \tau_1 = 0.355, \tau_2 = 0.495, \tau_3 = 5.32$ and assuming that $\varepsilon_{23} = \varepsilon_{32}$ and $\varepsilon_{12} = \varepsilon_{21}$ From eq. (4.7) & eq. (4.13),

$$\varepsilon_{32} = -(2\pi - 1.03 \times 6.17) \div \sin(1.03 \times 0.355) \tag{5.1}$$

$$\varepsilon_{32} = 0.2011 \sim 0.2 \tag{5.2}$$

$$\varepsilon_{12} = 0.1981 \sim 0.2 \tag{5.3}$$

Plugging ε_{32} as ε_{23} in eq. (4.11) we get,

$$\omega_2 T - \varepsilon_{21} \sin(\omega_2 \tau_2) - \varepsilon_{23} \sin(\omega_2(\tau_2 + \tau_3) - \varepsilon_{21} \sin(\omega_2 \tau_2)) = 6.2846 \sim 6.2832 \tag{5.4}$$

Putting $\varepsilon_{12} = \varepsilon_{21}$ in eq. (4.11),

$$\varepsilon_{23} = (\omega_2 T - \varepsilon_{21} \sin(\omega_2 \tau_2) - 2\pi) \div \sin(\omega_2(\tau_2 + \tau_3) - \varepsilon_{21} \sin(\omega_2 \tau_2)) \tag{5.5}$$

$\varepsilon_{23} = 0.1978$,which substituting in (2) gives 6.2844 (5.6)

5.1.2 3-unit oscillator with equal coupling strengths

Given (from XPP), $\omega_1 = \omega_2 = \omega_3 = 1, T = 6.3, \tau_1 = \tau_2 = \tau_3 = 2.1$ and $\varepsilon' s = 0.2$

$\phi_{21}^{'} = \omega\tau$ (From eq. (4.18))

$\phi_{21}^{'} = 1 \times 2.1$

$\phi_{21}^{'} = 2.1$ (5.7)

$\phi_{21} = \phi_{21}^{'} + \varepsilon \sin(\phi_{21}^{'})$ (From eq. (5.7))

$\phi_{21} = 2.1 + 0.2 \times \sin(2.1)$ (From eq. (4.18))

$\phi_{21} = 2.1 + 0.173$

$\phi_{21} = 2.273 \sim 2.277$ (5.8)

$\phi_{23}^{'} = \omega(\tau + \tau) + \varepsilon \sin(\phi_{21}^{'})$ (From eq. (5.8))

$\phi_{23}^{'} = 1 \times (2.1 + 2.1) + 0.2 \times \sin(2.1)$ (From eq. (4.18))

$\phi_{23}^{'} = 4.2 + 0.173$

$\phi_{23}^{'} = 4.373$ (5.9)

$\phi_{23} = \phi_{23}^{'} + \varepsilon \sin(\phi_{31}^{'})$ (From (18))

$\phi_{23} = 4.373 + 0.2 \times \sin(2.1) + 0.2 \times \sin(4.373)$ (From (20) & (22))

$\phi_{23} = 4.373 - 0.189$

$\phi_{23} = 4.184 \sim 4.189$ (5.10)

Plugging the values from (20) and (22) into the R.H.S of equation (19) we get,

R.H.S $= \omega T + \varepsilon \sin(\phi_{21}^{'}) + \varepsilon \sin(\phi_{31}^{'})$

R.H.S $= 1 \times 6.3 + 0.2 \times \sin(2.1) + 0.2 \times \sin(4.373)$

R.H.S $= 6.3 + 0.173 - 0.189$

R.H.S $= 6.28$

R.H.S $=$ L.H.S

5.1.3 4-unit oscillator with unknown value of third jump coupling strength

With $\tau = 1.6, \omega = 1,$ & $\varepsilon_1 = \varepsilon_2 = 0.2$, we search for a ε_3 satisfying eq. (4.22)

$$\phi_{24}^{'} = 1 \times 1.6$$
$$\phi_{24}^{'} = 1.6$$
$$\phi_{21}^{'} = 2 \times 1.6 + 0.2 \times \sin(1.6)$$
$$\phi_{21}^{'} = 3.4$$
$$\phi_{23}^{'} = 3 \times 1.6 + 0.2 \times \sin(1.6) + 0.2 \times \sin(3.4)$$
$$\phi_{23}^{'} = 4.95$$

According to eq. (4.22), 2π & ωT must be equal to the the total jumps

$$\begin{aligned}
\varepsilon_1 \sin(\phi_{24}^{'}) + \varepsilon_2 \sin(\phi_{21}^{'}) + \varepsilon_3 \sin(\phi_{23}^{'}) &= 2\pi - 1.6 \times 4 \\
\varepsilon_1 \sin(\phi_{24}^{'}) + \varepsilon_2 \sin(\phi_{21}^{'}) &= -0.12 - \varepsilon_3 \sin(\phi_{23}^{'}) \\
0.2 \times \sin(1.6) + 0.2 \times \sin(3.4) &= -0.12 - \varepsilon_3 \sin(4.95) \\
\varepsilon_3 &= -0.028 \div \sin(4.95) \\
\varepsilon_3 &= 0.27
\end{aligned}$$

Chapter 6

Results and Discussion

6.1 Spike train models

6.1.1 2-unit oscillator

We start with 2-unit oscillator where we test the all to all connected network with postive coupling, which is the easiest one to begin with as it has only 2-unit oscillators as shown in 6.1. We get an out-of-phase synchronization with the two oscillators and it was fairly resistant to the perturbations in the phases. This suggests that the reconstructed coupling strength for this network is likely to be accurate and reliable.

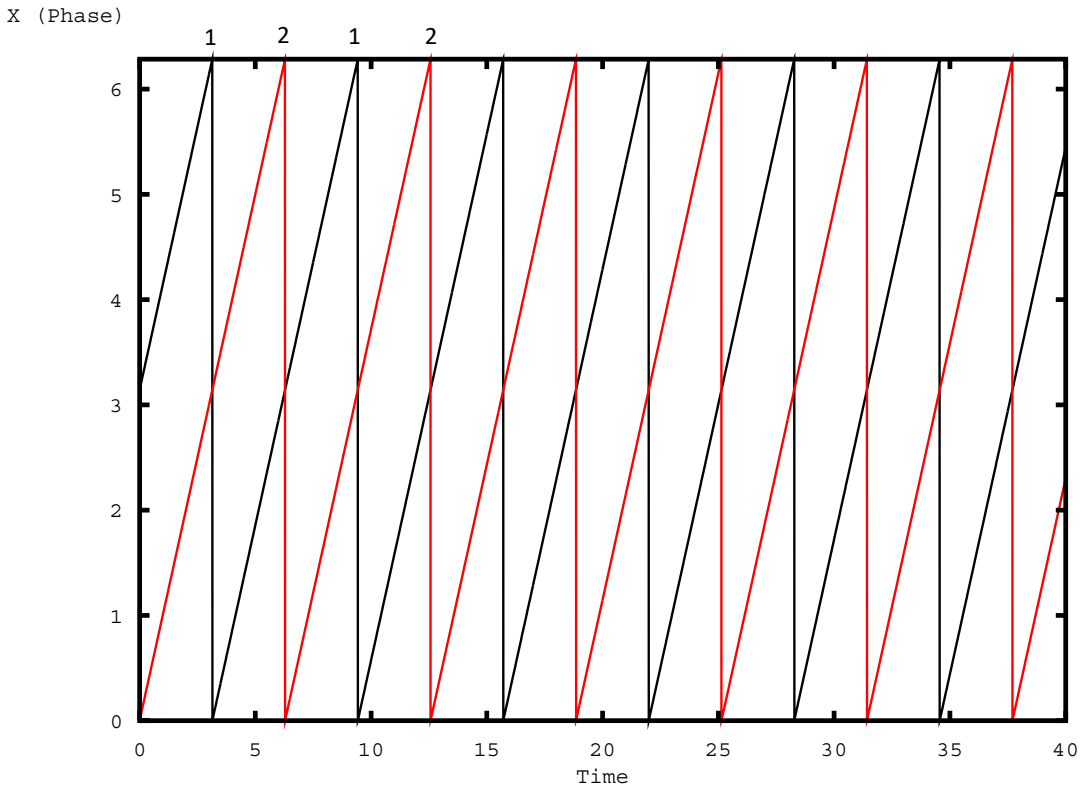

Figure 6.1: Phase time plot for the spike train model for 2-unit oscillators. Black Line represents unit 1 and red line represents unit 2. We get a perfect out-of-phase synchronization for the oscillators when the coupling is positive. The phases are initialized 2pi/2 apart, dt is 0.005, omega's are 1 and the coupling strengths are all equal to 0.2.

6.1.2 3-unit oscillator

We then moved on to add one more oscillator and tested the all-to-all connected 3-unit oscillator network with positive coupling. Similar to the 2-unit oscillator network, we observed that the system is stable with symmetric coupling globally, and the peaks of the neurons are 2pi/3 apart from each other, resulting in a synchronized and coherent system. To consider all possibilities, we made modifications to the all-to-all network as shown in 6.2a, 6.2b, and 6.2c. Furthermore, any perturbation in the system still leads to an out-of-phase

Nature of Coupling	**Coupling Strengths (ε)**	**Network Topology**	**Initial Phases**		**Observations**
			x_1	x_2	
Negative	0.2	1<->2	3.14	0	In-phase synchronization between the units 1 and 2, and a single peak
			1.2	6	Out-of-phase synchronization with the pattern: 1-2-1
Positive	0.2	1<->2	3.14	0	Out-of-phase synchronization with the pattern: 2-1-2
			1.2	6	Out-of-phase synchronization with the pattern: 2-1-2
		1->2	1.2	6	Out-of-phase synchronization with the pattern: 2-1-2
		2->1	1.2	6	

Table 6.1: Table showing the observations for the different topologies and patterns for the 2-unit oscillators

synchronized state, indicating a reliable model for reconstruction.

Firing Pattern		**Analytical Solution**					**XPP Values**	
	ε	$\phi_{23}^{'}$	$\phi_{21}^{'}$	**\eref{eq:2} RHS**	ϕ_{23}	ϕ_{21}	ϕ_{23}	ϕ_{21}
	0.2	2.1	4.373	6.284	2.273	4.184	2.273	4.184
1-2-3-1-2-3	0.1	2.095	4.277	6.281	2.181	4.186	2.185	4.189
	0.5	2.12	4.67	6.284	2.546	4.167	2.548	4.169
	ε	$\phi_{21}^{'}$	$\phi_{23}^{'}$	**\eref{eq:2} RHS**	ϕ_{21}	ϕ_{23}	ϕ_{21}	ϕ_{23}
	0.2	4.373	2.1	6.284	2.273	4.184	2.277	4.187
1-3-2-1-3-2	0.1	4.277	2.095	6.281	2.181	4.186	2.183	4.188
	0.5	4.67	2.12	6.284	2.546	4.167	2.542	4.167

Table 6.2: Table showing the stability of the phase equations with positive coupling with the help of 3 different coupling strengths for the 3-unit oscillator case

We observe that for both 2 and 3-unit oscillators, the system is stable with symmetric coupling globally and the peaks of the neurons are 2pi/(no. of unit oscillators) apart from each other. We also additionally checked the accuracy and stability of the 3-unit ocillator by trying different firing-patterns and coupling strengths (see table 6.2). This suggests that the system is synchronized and operating in a coherent manner. Also, any perturbation in the system (i.e., the peaks not being 2pi/(no. of unit oscillators apart) leads to the same out-of-phase synchronized state, and thus a reliable model for the reconstruction. The equally spaced peak distribution table for the 2 and 3-unit oscillator case is shown in table 6.1 and table 6.3 respectively.

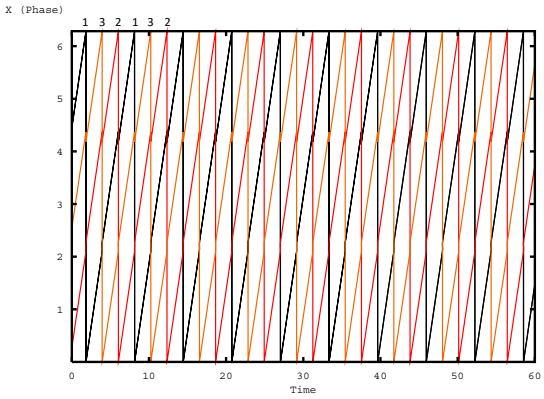

(a) The phases are initialized in the order 1->3->2. Here the pattern we get is 1-3-2-1-3-2.

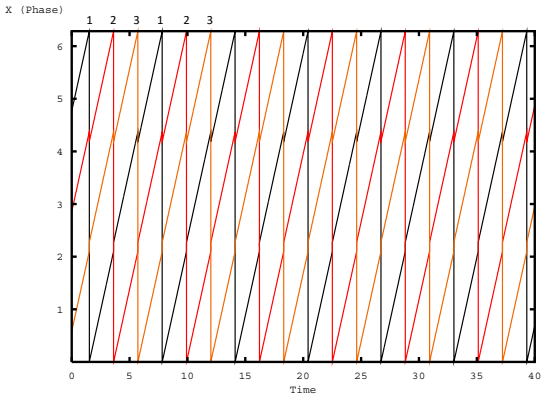

(b) The phases are initialized in the order 1->2->3. Here the pattern we get is 1-2-3-1-2-3.

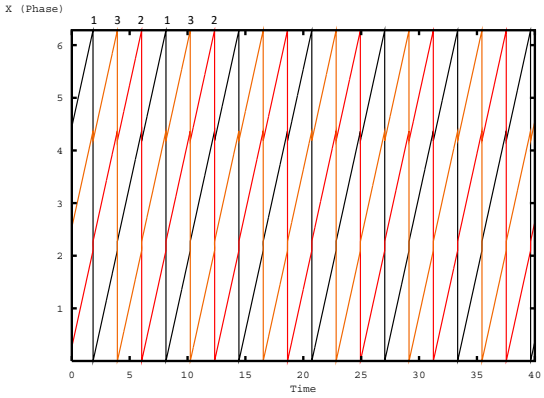

(c) The phases are initialized in the order 1->3->2. Here the pattern we get is 1-3-2-1-3-2.

Figure 6.2: Phase time plot for the spike train model for 3-unit oscillators and global (all-to-all) coupled network. The oscillators 1, 2, and 3 are indicated by the black, red, and orange lines respectively. The phases are initialized 2pi/3 apart, dt is 0.005, omega's are 1 and the coupling strengths are all equal to 0.2.

Nature of Coupling	**Coupling Strengths (ε)**	**Network Topology**	**Initial Phases**			**Observations**
			x_1	x_2	x_3	
Negative	0.2	All-to-all	4.189	2.094	0	In-phase synchronization between the units 1, 2, and 3 with a single peak
			5	3	0	
Positive	0.2	All-to-all	5	3	0	Out-of-phase synchronization with the pattern: 1-2-3-1
			5	0	3	Out-of-phase synchronization with the pattern: 1-3-2-1
		1->2->3->1	6	4	1	Out-of-phase synchronization with the pattern: 1-2-3-1
			6	1	4	Out-of-phase synchronization with the pattern: 1-3-2-1
		1->3->2->1	6	4	1	Out-of-phase synchronization with the pattern: 1-2-3-1
			6	1	4	Out-of-phase synchronization with the pattern: 1-3-2-1

Table 6.3: Table showing the observations for the different topologies and patterns for the 3-unit oscillators

6.1.3 4-unit oscillator

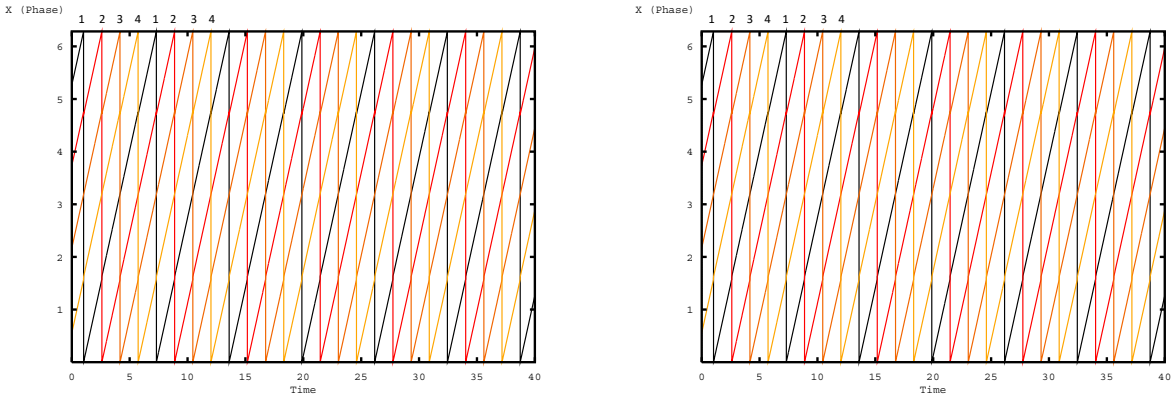

(a) The phases are initialized in the order 1->2->3->4. Here the pattern we get is 1-2-3-4-1-2-3-4.

(b) The phases are initialized in the order 1->2->3->4. Here the pattern we get is 1-2-3-4-1-2-3-4.

Figure 6.3: Phase time plot for the spike train model for 4-unit oscillators and global (all-to-all) coupled network. The oscillators 1, 2, 3, and 4 are indicated by the black, red, orange, and yellow lines respectively. The phases are initialized 2pi/4 apart, dt is 0.005, omega's are 1 and the coupling strengths are all equal to 0.05.

Nature of Coupling	Coupling Strengths (ε)	Network Topology	Initial Phases				Observations
			x_1	x_2	x_3	x_4	
Negative	0.02	All-to-all	4.713	3.142	0	1.571	In-phase synchronization between the units 1, 2, 3 and 4 with a single peak
Positive	0.05	All-to-all	4.713	3.142	1.571	0	Out-of-phase synchronization with the pattern: 1-2-3-4-1
	0.01		4.713	1.571	3.142	0	Out-of-phase synchronization with the pattern: 1-3-2-4-1
	0.02		4.713	0	3.142	1.571	Out-of-phase synchronization with the pattern: 1-3-4-2-1
			4.713	1.571	0	3.142	Out-of-phase synchronization with the pattern: 1-4-2-3-1
			4.713	0	1.571	3.142	Out-of-phase synchronization with the pattern: 1-4-3-2-1
			4.713	3.142	0	1.571	Out-of-phase synchronization with the pattern: 1-2-4-3-1
		1<->3<->2<->4<->1	4.713	1.571	3.142	0	Out-of-phase synchronization with the pattern: 1-3-2-4-1
			4.713	1.571	0	3.142	Out-of-phase synchronization with the pattern: 1-4-2-3-1
		1<->2<->3<->4<->1	4.713	3.142	1.571	0	Out-of-phase synchronization with the pattern: 1-2-3-4-1
			4.713	0	1.571	3.142	Out-of-phase synchronization with the pattern: 1-4-3-2-1
		1<->2<->4<->3<->1	4.713	3.142	0	1.571	Out-of-phase synchronization with the pattern: 1-2-4-3-1
			4.713	0	3.142	1.571	Out-of-phase synchronization with the pattern: 1-3-4-2-1
		1->3->2->4->1	4.713	1.571	3.142	0	Out-of-phase synchronization with the pattern: 1-3-2-4-1
			4.713	1.571	0	3.142	Out-of-phase synchronization with the pattern: 1-4-2-3-1
		1->2->3->4->1	4.713	3.142	1.571	0	Out-of-phase synchronization with the pattern: 1-2-3-4-1
			4.713	0	1.571	3.142	Out-of-phase synchronization with the pattern: 1-4-3-2-1
		1->2->4->3->1	4.713	3.142	0	1.571	Out-of-phase synchronization with the pattern: 1-2-4-3-1
			4.713	0	3.142	1.571	Out-of-phase synchronization with the pattern: 1-3-4-2-1

Table 6.4: Table showing the observations for the different topologies and patterns for the 4-unit oscillators

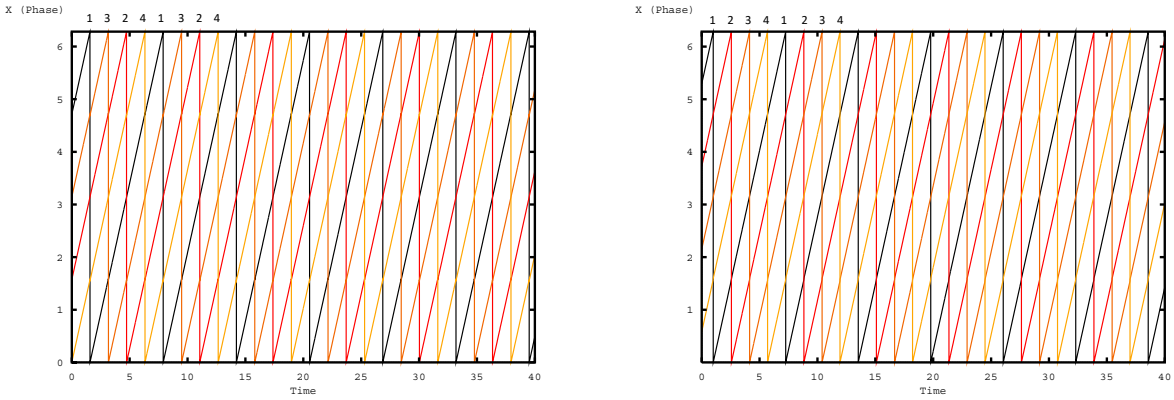

(a) The phases are initialized in the order 1<->3<->2<->4<->1. Here the pattern we get is 1-3-2-4-1-3-2-4.

(b) The phases are initialized in the order 1<->2<->3<->4<->1. Here the pattern we get is 1-2-3-4-1-2-3-4.

Figure 6.4: Phase time plot for the spike train model for 4-unit oscillators which are bidirectionally chain coupled. The oscillators 1, 2, 3, and 4 are indicated by the black, red, orange, and yellow lines respectively. The phases are initialized 2pi/4 apart, dt is 0.005, omega's are 1 and the coupling strengths are all equal to 0.02.

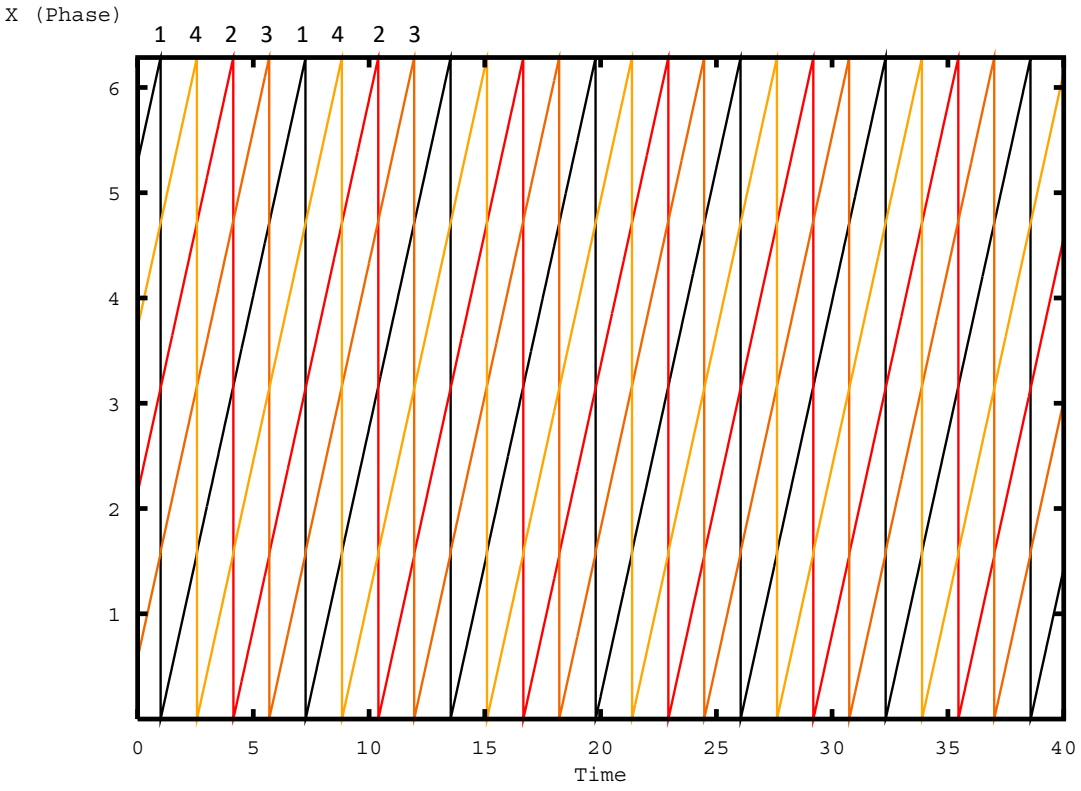

Figure 6.5: Phase time plot for the spike train model for 4-unit oscillators which are bidirectionally chain coupled. The oscillators 1, 2, 3, and 4 are indicated by the black, red, orange, and yellow lines respectively. The phases are initialized 2pi/4 apart, and in the order 1<->4<->2<->3<->1, dt is 0.005, omega's are 1 and the coupling strengths are all equal to 0.02. Here the pattern we get is 1-4-2-3-1-4-2-3.

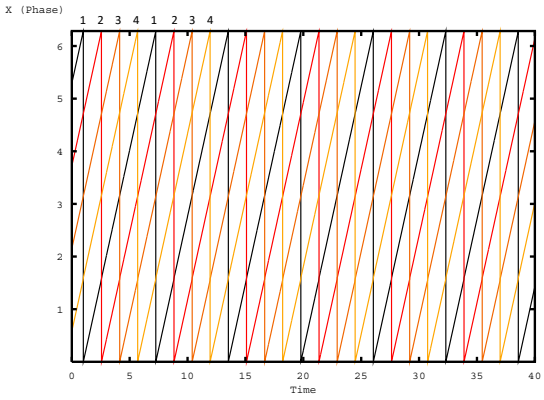

(a) The phases are initialized in the order 1->2->3->4->1. Here the pattern we get is 1-2-3-4-1-2-3-4.

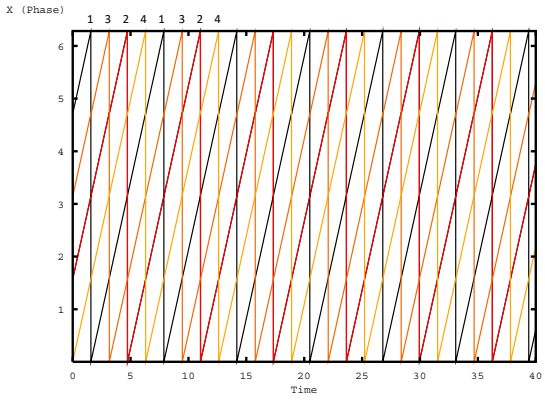

(b) The phases are initialized in the order 1->3->2->4->1. Here the pattern we get is 1-3-2-4-1-3-2-4.

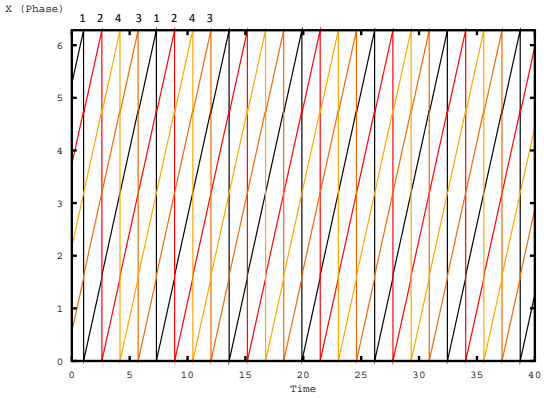

(c) The phases are initialized in the order 1->2->4->3->1. Here the pattern we get is 1-2-4-3-1-2-4-3.

Figure 6.6: Phase time plot for the spike train model for 4-unit oscillators which are unidirectionally chain coupled. The oscillators 1, 2, 3, and 4 are indicated by the black, red, orange, and yellow lines respectively. The phases are initialized 2pi/4 apart, dt is 0.005, omega's are 1 and the coupling strengths are all equal to 0.02.

6.1.4 5-unit oscillator

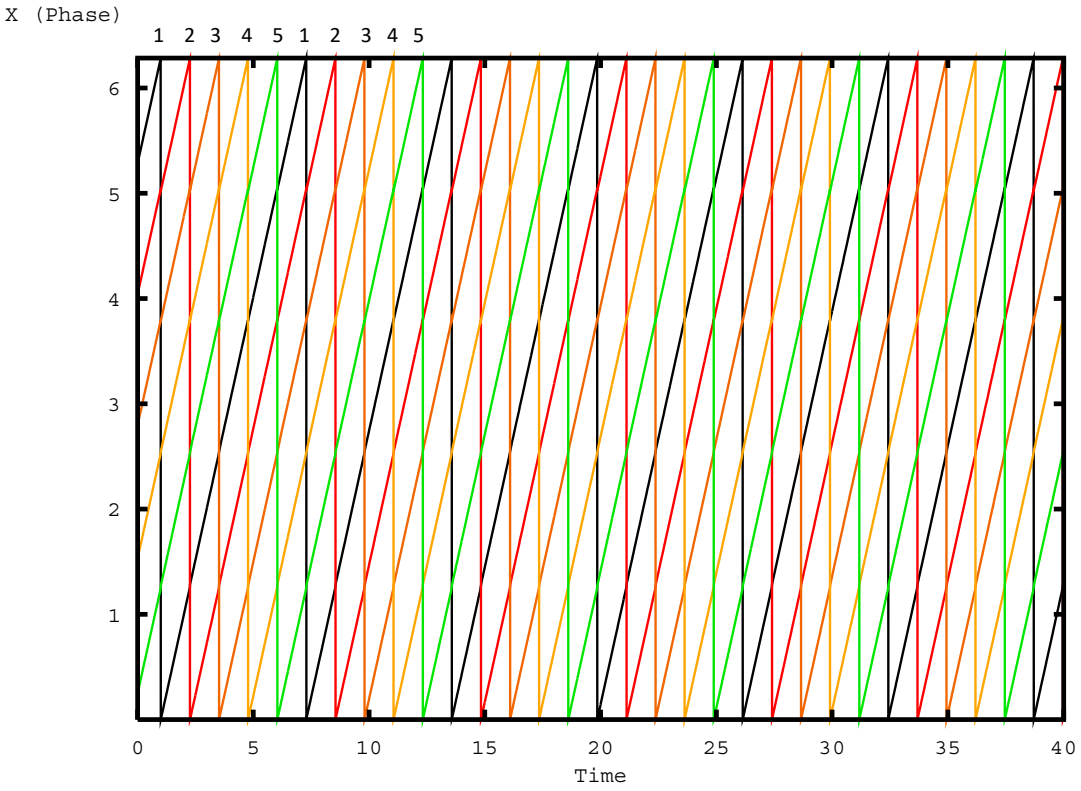

Figure 6.7: Phase time plot for the spike train model for 5-unit oscillators which are unidirectionally chain coupled. The oscillators 1, 2, 3, 4, and 5 are indicated by the black, red, orange, yellow, and green lines respectively. The phases are initialized 2pi/5 apart, and in the order 1->2->4->3->1, dt is 0.005, omega's are 1 and the coupling strengths are all equal to 0.02. Here the pattern we get is 1-2-3-4-5-1-2-3-4-5.

For the 4 and 5-unit case, the globally-coupled oscillator case(figs. 6.3a and 6.3b and fig. 6.7), and all the variations shown in fig. 6.4a through fig. 6.6c, we observe for that, when initiated 2pi/(no. of unit oscillators) apart, the system runs on to be out-of-phase synchronized. But when the system is perturbed, the oscillators merge and synchronize with each other making reconstruction impossible. This means that while the equally spaced peaks is one of the solution for the problem, it is not a stable one.

Nature of Coupling	Coupling Strengths (ε)	Network Topology	Initial Phases					Observations
			x_1	x_2	x_3	x_4	x_5	
Negative	0.02	All-to-all	5.027	3.77	2.513	1.257	0	In-phase synchronization between the units 1, 2, 3, 4 and 5 with a single peak
Positive		All-to-all	5.027	3.77	2.513	1.257	0	Out-of-phase synchronization with the pattern: 1-2-3-4-5-1
			5.027	3.77	2.513	0	1.257	Out-of-phase synchronization with the pattern: 1-2-3-5-4-1
			5.027	3.77	1.257	2.513	0	Out-of-phase synchronization with the pattern: 1-2-4-3-5
			5.027	3.77	0	2.513	1.257	Out-of-phase synchronization with the pattern: 1-2-4-5-3-1
			5.027	3.77	1.257	0	2.513	Out-of-phase synchronization with the pattern: 1-2-5-3-4-1
			5.027	3.77	0	1.257	2.513	Out-of-phase synchronization with the pattern: 1-2-5-4-3-1
			5.027	2.513	3.77	1.257	0	Out-of-phase synchronization with the pattern: 1-3-2-4-5-1

Table 6.5: Table showing the observations for the different topologies and patterns for the 5-unit oscillators, Part 1

Nature of Coupling	Coupling Strengths (ε)	Network Topology	Initial Phases					Observations
			x_1	x_2	x_3	x_4	x_5	
Positive	0.02	All-to-all	5.027	2.513	3.77	0	1.257	Out-of-phase synchronization with the pattern: 1-3-2-5-4-1
			5.027	1.257	3.77	2.513	0	Out-of-phase synchronization with the pattern: 1-3-4-2-5-1
			5.027	0	3.77	2.513	1.257	Out-of-phase synchronization with the pattern: 1-3-4-5-2-1
			5.027	1.257	3.77	0	2.513	Out-of-phase synchronization with the pattern: 1-3-5-2-4-1
			5.027	0	3.77	1.257	2.513	Out-of-phase synchronization with the pattern: 1-3-5-4-2-1
			5.027	2.513	1.257	3.77	0	Out-of-phase synchronization with the pattern: 1-4-2-3-5-1
			5.027	2.513	0	3.77	1.257	Out-of-phase synchronization with the pattern: 1-4-2-5-3-1
			5.027	1.257	2.513	3.77	0	Out-of-phase synchronization with the pattern: 1-4-3-2-5-1

Table 6.6: Table showing the observations for the different topologies and patterns for the 5-unit oscillators, Part 2

Nature of Coupling	Coupling Strengths (ε)	Network Topology	Initial Phases					Observations
			x_1	x_2	x_3	x_4	x_5	
Positive	0.02	All-to-all	5.027	0	2.513	3.77	1.257	Out-of-phase synchronization with the pattern: 1-4-3-5-2-1
			5.027	1.257	0	3.77	2.513	Out-of-phase synchronization with the pattern: 1-4-5-2-3-1
			5.027	0	1.257	3.77	2.513	Out-of-phase synchronization with the pattern: 1-4-5-3-2-1
			5.027	2.513	1.257	0	3.77	Out-of-phase synchronization with the pattern: 1-5-2-3-4-1
			5.027	2.513	0	1.257	3.77	Out-of-phase synchronization with the pattern: 1-5-2-4-3-1
			5.027	1.257	0	2.513	3.77	Out-of-phase synchronization with the pattern: 1-5-4-2-3-1
			5.027	0	1.257	2.513	3.77	Out-of-phase synchronization with the pattern: 1-5-4-3-2-1
			5.027	1.257	2.513	0	3.77	Out-of-phase synchronization with the pattern: 1-5-3-2-4-1
			5.027	0	2.513	1.257	3.77	Out-of-phase synchronization with the pattern: 1-5-3-4-2-1

Table 6.7: Observations for 5-unit oscillators, Part 3

Nature of Coupling	Coupling Strengths (ε)	Network Topology	Initial Phases					Observations
			x_1	x_2	x_3	x_4	x_5	
Positive	0.02	1->2->3->4->5->1	5.027	3.77	2.513	1.257	0	Out-of-phase synchronization with the pattern: 1-2-3-4-5-1
			5.027	0	1.257	2.513	3.77	Out-of-phase synchronization with the pattern: 1-5-4-3-2-1
		1<->2<->3<->4<->5<->1	5.027	3.77	2.513	1.257	0	Out-of-phase synchronization with the pattern: 1-3-5-2-4-1
			5.027	1.257	3.77	0	2.513	Out-of-phase synchronization with the pattern: 1-3-5-2-4-1
			5.027	3.77	2.513	1.257	0	Out-of-phase synchronization with the pattern: 1-4-2-5-3-1
			5.027	2.513	0	3.77	1.257	Out-of-phase synchronization with the pattern: 1-4-2-5-3-1

Table 6.8: Table showing the observations for the different topologies and patterns for the 5-unit oscillators, Part 4

We still do not have a plausible explanation for this behavior exhibited by the model where the units greater than 4 only had one possible stable equally peaked synchronized solution. Also, for the 5-unit uni-directional and bi-directional chain cases, there was an anomaly observed where the chain 1 through 5 didn't result in an equally spaced synchronized state for the firing pattern 1->2->3->4->5, but some different firing pattern. This gives us an idea about the complexity of the underlying network where even if the units are not connected, the firing pattern is reflected.

Chapter 7

Conclusion

Starting with the Kuramoto model for studying the reconstruction of the coupling strengths of the oscillators using the time series data and Van der Pol as the intrinsic dynamics of the oscillator, we learned that the model is great for 2 unit oscillators, but as the system complexity increases the model becomes computationally intensive, and the accuracy of reconstruction decreases. Moving on to the spike train models, while we do get additional stability with the case of the 2 and 3-unit oscillator, the spike train model does not provide a solution for the coupling reconstruction problem when the number of oscillators increases further, which shows that there is still room for further research and development in this area, with the aim of finding more efficient and accurate methods for reconstructing coupling strengths in complex oscillator systems.

The observations suggest that the synchronization of oscillators in all-to-all connected networks with positive coupling is dependent on the number of oscillators in the network. The experiment began with a 2-unit oscillator network that exhibited an out-of-phase synchronization with the two oscillators. This synchronization was found to be resistant to perturbations, indicating that the reconstructed coupling strength for this network is likely to be accurate and reliable. Moving on to a 3-unit oscillator network, we observed that the system was stable with symmetric coupling globally, and the peaks of the neurons were $2\pi/3$ apart from each other. This resulted in a synchronized and coherent system. Furthermore, any perturbation in the system still led to an out-of-phase synchronized state, indicating that the model was reliable for reconstruction. To consider all possibili-

ties, modifications were made to the all-to-all network by varying the coupling strengths and introducing phase shifts between the oscillators. However, even with these modifications, the system remained stable, indicating that the synchronization observed was robust and not dependent on the specific network topology. However, for the 4 and 5-unit oscillator networks, the researchers observed that although the system ran on to be out-of-phase synchronized when initiated 2π/(no. of unit oscillators) apart, any perturbation led to the synchronization of the oscillators, making reconstruction impossible. This meant that equally spaced peaks while being one of the possible stable solutions for the problem was not a fully stable case where it was robust to the perturbations. Overall, the observations suggest that the synchronization of oscillators in all-to-all connected networks with positive coupling is a complex phenomenon that is dependent on the number of oscillators in the network and the specific network topology. The findings also highlight the importance of considering different network topologies to determine the reliable reconstruction of coupling strength.

All the findings where the all-to-all stable pattern is generated give a nice baseline of a model to start finding links about how the working memory actually could function in chimpanzees. The all-to-all network topology also fits in correctly intuition wise where any sequence given to the chimpanzee can be memorized and recalled in any order, which is reminiscent of an all-to-all network where there are equal interactions between all neurons. But the chain coupled cases also showed unpredictable, but promising where if a unit corresponding to a certain numeral isn't even connected topology-wise to another unit, it can still generate a particular pattern, which could be hypothesized to be a plastic neural network. Further research is needed to determine the extent to which these findings apply to real-world neural networks and working memory in chimpanzees. One of the most key takeaways from this work is that as the complexity of the system increases in terms of the number of unit oscillators, the coupling strength has to decrease almost as if to accommodate the increased number of resulting patterns between the units. We can hypothesize that this is an attribute that could be restricted to young chimpanzees and gets lost in humans with time. While this hypothesis may be plausible, it is essential to note that further research would need to be conducted to determine if the observed relationship between system complexity and coupling strength is indeed present in other species and maintained throughout development.

Chapter 8

Appendix

8.1 MATLAB code for reconstructing the coupling strength from the simulated data for the Van der Pol oscillator

Code 8.1: MATLAB code for reconstructing coupling strengths with minimization applied.

```
1   function Timeseries_to_CouplingStrengthReconstruction_Manual =
        do_it(tab, ...
2   u1, u2)
3
4   % Preprocessing the tabular data (tab) in the format of x1,y1,x2,y2
        wrt
5   % time, where u1 and u2 are the damping coefficients.
6   % Creating variables from the table and fetching the column length
        of
7   % the table,
8   % s (height) of the tabular matrix is calcualted to get the number
        of
9   % iterates
10  Time = tab.Time;
11  x1 = tab.x1;
12  x2 = tab.x2;
13  y1 = tab.y2;
```

```
14      y2 = tab.y2;
15      s = height(tab);
16
17      % x1D and x2D: Derivatives of the 2 unit oscillators. A zero array
            of
18      % required size initiated before every calculation to ease and
            hasten
19      % the computation as matlab uses more resources if the arrays are
20      % initiated and concatenated while computing.
21      x1D = zeros([s 1]);
22      x2D = zeros([s 1]);
23      for i = 2:s
24          x1D(i) = (x1(i)-x1(i-1))/(Time(i)-Time(i-1));
25          x2D(i) = (x2(i)-x2(i-1))/(Time(i)-Time(i-1));
26      end
27
28      % X1 and X2: LHS of the matrix equation [equation (3), equation box
            2]
29      X1 = zeros([s 1]);
30      X2 = zeros([s 1]);
31      for i = 2:s
32          X1(i) = x1D(i)-u1*(x1(i)-(1/3)*x1(i).^3-y1(i));
33          X2(i) = x2D(i)-u2*(x2(i)-(1/3)*x2(i).^3-y2(i));
34      end
35
36      % g12 and g21: Coupling functions calculated as a function of the
37      % phases
38      g12 = zeros([s 1]);
39      g21 = zeros([s 1]);
40      for i = 2:s
41          g12(i) = x1(i)-x2(i);
42          g21(i) = x2(i)-x1(i);
43      end
44
45      % Minimization to the coupling strength, individual terms
            calculated
46      % from the general formula derived by applying minimization:
```

```
    % J12 = [(X1,1*g12,1/a) + (X1,2*g12,2/a) + (X1,3*g12,3/a) + ...)]
    % Where a = (g12,1^2 + g12,2^2 + g12,3^2 + ...)
    % gsqr is the individual terms raised to the power of two and den
       is
    % the denominator of the equation (7), equation box 3.

    % Calculating a
    gsqr = g12.^2;
    den = sum(gsqr);

    % Calculating the different numerators for the different coupling
    % strengths (J12 and J21): num1 and num2
    num1 = zeros([s 1]);
    num2 = zeros([s 1]);
    for i = 2:s
        num1(i) = X1(i)*g12(i)/den;
        num2(i) = X2(i)*g21(i)/den;
    end

    % J1 and J2: Reconstructed coupling strengths
    J1 = sum(num1);
    J2 = sum(num2);

    Timeseries_to_CouplingStrengthReconstruction_Manual = [J1, J2];
    end
```

8.2 ODE files used to simulate Van der pol model

Code 8.2: Van der pol equation ODE file for 2-unit oscillator.

```
    # van der Pol for 2 unit oscillator - coupled

    x1'=y1+a11*(x1-x1)+a12*(x1-x2)
    y1'=-x1+y1*u*(1-x1^2)

```

```
    x2'=y2+a21*(x2-x1)+a22*(x2-x2)
    y2'=-x2+y2*e*(1-x2^2)

    init x1=1,x2=1,y1=1,y2=1
    par u=.8,e=.6,a11=0,a12=1,a22=0,a21=1
    @ method=cvode,total=500, dt=0.005

    done
```

8.3 ODE files used to simulate spike train models

8.3.1 2-unit oscillator

8.3.1.1

Code 8.3: Spike train equation ODE file for 2-unit oscillator with positive global coupling.

```
            #2-unit postive coupling (e = 0.2)
            #Equations for the globally coupled oscillator for 2 units
               with positive coupling strengths. Here both the units
               are connected to each other.
          #Parameters: All coupling strengths (e) are equal to 0.2 and
             omeaga's (w) are equal to 1
          #Initial Condition: The phases are kept (2*pi)/2 apart

            x1' = w1
            x2' = w2

            global 1 x1-2*pi {x1=0;x2=x2+e21*sin(x2)}
            global 1 x2-2*pi {x2=0;x1=x1+e12*sin(x1)}
            init x1=3.14,x2=0
            par w1=1,w2=1,e21=0.2,e12=0.2

            @ method=cvode,total=500, dt=0.005
```

```
15            done
```

8.3.1.2

Code 8.4: Spike train equation ODE file for 2-unit oscillator with negative global coupling.

```
1             #2-unit negative coupling (e = 0.2)
2             #Equations for the globally coupled oscillator for 2 units
                 with negative coupling strengths. Here both the units
                 are connected to each other.
3           #Parameters: All coupling strengths (e) are equal to 0.2 and
               omeaga's (w) are equal to 1
4           #Initial Condition: The phases are kept (2*pi)/2 apart
5
6             x1' = w1
7             x2' = w2
8
9             global 1 x1-2*pi {x1=0;x2=x2-e21*sin(x2)}
10            global 1 x2-2*pi {x2=0;x1=x1-e12*sin(x1)}
11
12            init x1=3.14,x2=0
13            par w1=1,w2=1,e21=0.2,e12=0.2
14            @ method=cvode,total=500, dt=0.005
15
16            done
```

8.3.2 3-unit oscillator

8.3.2.1

Code 8.5: Spike train equation ODE file for 3-unit oscillator with positive global coupling.

```
1             #Equations for the globally coupled oscillator for 2 units
                 with positive coupling strengths.
```

```
#Parameters: All coupling strengths (e) are equal to 0.2 and
   omeaga's (w) are equal to 1
#Initial Condition: The phases are kept (2*pi)/3 apart
  # 3-unit global coupling (e=0.2)

  x1' = w1
  x2' = w2
  x3' = w3

  global 1 x1-2*pi {x1=0;x2=x2+e21*sin(x2);x3=x3+e31*sin(x3)}
  global 1 x2-2*pi {x2=0;x3=x3+e32*sin(x3);x1=x1+e12*sin(x1)}
  global 1 x3-2*pi {x3=0;x2=x2+e23*sin(x2);x1=x1+e13*sin(x1)}

  init x1=4.188,x2=2.094,x3=0
  par w1=1,w2=1,w3=1,e21=0.2,e32=0.2,e12=0.2,e23=0.2,e13=0.2,
     e31=0.2
  @ method=cvode,total=500, dt=0.005

  done
```

8.3.2.2

Code 8.6: Spike train equation ODE file for 3-unit oscillator with chained unidirectional coupling (pattern 1).

```
  #Equations for the chained unidirectionally coupled
     oscillator, where 1->2->3->1 (e21,e32,e13)
#Parameters: All coupling strengths (e) are equal to 0.2 and
   omeaga's (w) are equal to 1
#Initial Condition: The phases are kept (2*pi)/3 apart
  # 3-unit chain-coupled (1-2-3-1-)

  x1' = w1
  x2' = w2
  x3' = w3

```

```
            global 1 x1-2*pi {x1=0;x2=x2+e21*sin(x2)}
            global 1 x2-2*pi {x2=0;x3=x3+e32*sin(x3)}
            global 1 x3-2*pi {x3=0;x1=x1+e13*sin(x1)}

            init x1=4.188,x2=2.094,x3=0
            par w1=1,w2=1,w3=1,e21=0.2,e32=0.2,e12=0.2,e23=0.2,e13=0.2,
               e31=0.2
            @ method=cvode,total=500, dt=0.005

            done
```

8.3.2.3

Code 8.7: Spike train equation ODE file for 3-unit oscillator with chained unidirectional coupling (pattern 2).

```
            #Equations for the chained unidirectionally coupled
               oscillator, where 1->3->2->1 (e31,e23,e12)
          #Parameters: All coupling strengths (e) are equal to 0.2 and
             omeaga's (w) are equal to 1
          #Initial Condition: The phases are kept (2*pi)/3 apart
            # 3-unit chain-coupled (1-3-2-1-)

            x1' = w1
            x2' = w2
            x3' = w3

            global 1 x1-2*pi {x1=0;x3=x3+e31*sin(x3)}
            global 1 x2-2*pi {x2=0;x1=x1+e12*sin(x1)}
            global 1 x3-2*pi {x3=0;x2=x2+e23*sin(x2)}

            init x1=4.188,x2=2.094,x3=0
            par w1=1,w2=1,w3=1,e21=0.2,e32=0.2,e12=0.2,e23=0.2,e13=0.2,
               e31=0.2
            @ method=cvode,total=500, dt=0.005

```

```
18            done
```

8.3.2.4

Code 8.8: Spike train equation ODE file for 3-unit oscillator with bidirectional coupling.

```
1             #Equations for the bidirectional coupled oscillator, where
                 1<->2<->3 (e12,e21,e23,e32)
2           #Parameters: All coupling strengths (e) are equal to 0.2 and
                omeaga's (w) are equal to 1
3           #Initial Condition: The phases are kept (2*pi)/3 apart
4             # 3-unit birectional chain coupling (1=2=3)
5
6             x1' = w1
7             x2' = w2
8             x3' = w3
9
10            global 1 x1-2*pi {x1=0;x2=x2+e21*sin(x2)}
11            global 1 x2-2*pi {x2=0;x3=x3+e32*sin(x3);x1=x1+e12*sin(x1)}
12            global 1 x3-2*pi {x3=0;x2=x2+e23*sin(x2)}
13
14            init x1=4.188,x2=2.094,x3=0
15            par w1=1,w2=1,w3=1,e21=0.2,e32=0.2,e12=0.2,e23=0.2,e13=0.2,
                 e31=0.2
16            @ method=cvode,total=500, dt=0.005
17
18            done
```

8.3.3 4-unit oscillator

8.3.3.1

Code 8.9: Spike train equation ODE file for 4-unit oscillator with postive global coupling.

```
#Equations for the globally coupled oscillator for 4 units with positive coupling strengths.
#Parameters: All coupling strengths (e) are equal to 0.05 and omeaga's (w) are equal to 1
#Initial Condition: The phases are kept (2*pi)/4 apart
# 4-unit global (e = 0.05)

x1' = w1
x2' = w2
x3' = w3
x4' = w4

global 1 x1-2*pi {x1=0;x2=x2+e21*sin(x2);x3=x3+e31*sin(x3);x4=x4+e41*sin(x4)}
global 1 x2-2*pi {x2=0;x3=x3+e32*sin(x3);x1=x1+e12*sin(x1);x4=x4+e42*sin(x4)}
global 1 x3-2*pi {x3=0;x2=x2+e23*sin(x2);x1=x1+e13*sin(x1);x4=x4+e43*sin(x4)}
global 1 x4-2*pi {x4=0;x2=x2+e24*sin(x2);x1=x1+e14*sin(x1);x3=x3+e34*sin(x3)}

init x1=4.713,x2=3.142,x3=1.571,x4=0
par w1=1,w2=1,w3=1,w4=1,e21=0.05,e32=0.05,e12=0.05,e23=0.05,e13=0.05,e31=0.05,e24=0.05,e14=0.05,e34=0.05,e41=0.05,e42=0.05,e43=0.05
@ method=cvode,total=500, dt=0.005

done
```

8.3.3.2

Code 8.10: Spike train equation ODE file for 4-unit oscillator with bidirectional coupling.

```
#Equations for the bidirectionally chain coupled oscillator where 1<->3<->2<->4<->1 (e13,e31,e32,e23,e24,e42,e41,e14)
```

```
2           #Parameters: All coupling strengths (e) are equal to 0.02 and
                omeaga's (w) are equal to 1
3           #Initial Condition: The phases are kept (2*pi)/4 apart
4             # 4-unit 1-3-2-4-1 bidirectional chain (e=0.02)
5
6             x1' = w1
7             x2' = w2
8             x3' = w3
9             x4' = w4
10
11            global 1 x1-2*pi {x1=0;x3=x3+e31*sin(x3);x4=x4+e41*sin(x4)}
12            global 1 x2-2*pi {x2=0;x3=x3+e32*sin(x3);x4=x4+e42*sin(x4)}
13            global 1 x3-2*pi {x3=0;x2=x2+e23*sin(x2);x1=x1+e13*sin(x1)}
14            global 1 x4-2*pi {x4=0;x2=x2+e24*sin(x2);x1=x1+e14*sin(x1)}
15
16            init x1=4.71,x2=1.57,x3=3.14,x4=0
17            par w1=1,w2=1,w3=1,w4=1,e21=0.02,e32=0.02,e12=0.02,e13
                 =0.02,e24=0.02,e34=0.02,e41=0.02,e43=0.02,e23=0.02,e14
                 =0.02,e31=0.02,e42=0.02
18            @ method=cvode,total=500, dt=0.005
19
20            done
```

8.3.3.3

Code 8.11: Spike train equation ODE file for 4-unit oscillator with unidirectional chain coupling.

```
1             #Equations for the unidirectionally chain coupled
                 oscillator where 1->2->3->4->1 (e21,e32,e43,e14)
2           #Parameters: All coupling strengths (e) are equal to 0.02 and
                omeaga's (w) are equal to 1
3           #Initial Condition: The phases are kept (2*pi)/4 apart
4             # 4-unit 1-2-3-4-1 unidirectional coupling (e=0.02)
5
6             x1' = w1
```

```
7             x2' = w2
8             x3' = w3
9             x4' = w4
10
11            global 1 x1-2*pi {x1=0;x2=x2+e21*sin(x2)}
12            global 1 x2-2*pi {x2=0;x3=x3+e32*sin(x3)}
13            global 1 x3-2*pi {x3=0;x4=x4+e43*sin(x4)}
14            global 1 x4-2*pi {x4=0;x1=x1+e14*sin(x1)}
15
16            init x1=4.71,x2=3.14,x3=1.57,x4=0
17            par w1=1,w2=1,w3=1,w4=1,e21=0.02,e32=0.02,e12=0.02,e13
                 =0.02,e24=0.02,e34=0.02,e41=0.02,e43=0.02,e23=0.02,e14
                 =0.02,e31=0.02,e42=0.02
18            @ method=cvode,total=500, dt=0.005
19
20            done
```

8.3.4 5-unit oscillator

Code 8.12: Spike train equation ODE file for 5-unit oscillator with global positive coupling.

```
1         # 5-unit e = 0.02
2
3         x1' = w1
4         x2' = w2
5         x3' = w3
6         x4' = w4
7         x5' = w5
8
9         global 1 x1-2*pi {x1=0;x2=x2+e21*sin(x2);x3=x3+e31*sin(x3);x4=
             x4+e41*sin(x4);x5=x5+e51*sin(x5)}
10        global 1 x2-2*pi {x2=0;x3=x3+e32*sin(x3);x1=x1+e12*sin(x1);x4=
             x4+e42*sin(x4);x5=x5+e52*sin(x5)}
11        global 1 x3-2*pi {x3=0;x2=x2+e23*sin(x2);x1=x1+e13*sin(x1);x4=
             x4+e43*sin(x4);x5=x5+e53*sin(x5)}
```

```
12        global 1 x4-2*pi {x4=0;x2=x2+e24*sin(x2);x1=x1+e14*sin(x1);x3=
             x3+e34*sin(x3);x5=x5+e54*sin(x5)}
13        global 1 x5-2*pi {x5=0;x2=x2+e25*sin(x2);x1=x1+e15*sin(x1);x3=
             x3+e35*sin(x3);x4=x4+e45*sin(x4)}
14
15        init x1=5.027,x2=3.77,x3=2.513,x4=1.257,x5=0
16        par w1=1,w2=1,w3=1,w4=1,w5=1,e21=0.02,e32=0.02,e12=0.02,e23
             =0.02,e13=0.02,e31=0.02,e24=0.02,e14=0.02,e34=0.02,e41=0.02,
             e42=0.02,e43=0.02,e45=0.02,e51=0.02,e52=0.02,e53=0.02,e54
             =0.02,e15=0.02,e25=0.02,e35=0.02
17        @ method=cvode,total=80, dt=0.005
18
19        done
```

Github repository link with all ODE files: `https://github.com/goelpranay/SuyogSankheThesis.git`

References

Baddeley, A. D., & Hitch, G. (1974). Working memory. In *Psychology of learning and motivation* (pp. 47–89). Elsevier. Retrieved from https://doi.org/10.1016%2Fs0079-7421%2808%2960452-1 doi: 10.1016/s0079-7421(08)60452-1

Cantwell, A., Buckholtz, J. W., Atencia, R., & Rosati, A. G. (2022, may). The origins of cognitive flexibility in chimpanzees. *Developmental Science*, *25*(5). Retrieved from https://doi.org/10.1111%2Fdesc.13266 doi: 10.1111/desc.13266

Cestnik, R., & Rosenblum, M. (2017, jul). Reconstructing networks of pulse-coupled oscillators from spike trains. *Physical Review E*, *96*(1). Retrieved from https://doi.org/10.1103%2Fphysreve.96.012209 doi: 10.1103/physreve.96.012209

Chai, W. J., Hamid, A. I. A., & Abdullah, J. M. (2018, mar). Working memory from the psychological and neurosciences perspectives: A review. *Frontiers in Psychology*, *9*. Retrieved from https://doi.org/10.3389%2Ffpsyg.2018.00401 doi: 10.3389/fpsyg.2018.00401

Compte, A. (2000, sep). Synaptic mechanisms and network dynamics underlying spatial working memory in a cortical network model. *Cerebral Cortex*, *10*(9), 910–923. Retrieved from https://doi.org/10.1093%2Fcercor%2F10.9.910 doi: 10.1093/cercor/10.9.910

Constantinidis, C., & Klingberg, T. (2016, may). The neuroscience of working memory capacity and training. *Nature Reviews Neuroscience*, *17*(7), 438–449. Retrieved from https://doi.org/10.1038%2Fnrn.2016.43 doi: 10.1038/nrn.2016.43

Cowan, N. (2001, feb). The magical number 4 in short-term memory: A reconsideration of mental storage capacity. *Behavioral and Brain Sciences*, *24*(1), 87–114. Retrieved from https://doi.org/10.1017%2Fs0140525x01003922 doi: 10.1017/s0140525x01003922

Ermentrout, B. (2007). XPPAUT. *Scholarpedia*, *2*(1), 1399. Retrieved from https://doi.org/10.4249%2Fscholarpedia.1399 doi: 10.4249/scholarpedia.1399

Guo, Y., Zhang, D., Li, Z., Wang, Q., & Yu, D. (2021, jul). Overviews on the applications of the kuramoto model in modern power system analysis. *International Journal of Electrical Power &amp Energy Systems*, *129*, 106804. Retrieved from https://doi.org/10.1016%2Fj.ijepes.2021.106804 doi: 10.1016/j.ijepes.2021.106804

Herrmann, E., Call, J., Hernańdez-Lloreda, M. V., Hare, B., & Tomasello, M. (2007, sep). Humans have evolved specialized skills of social cognition: The cultural intelligence

hypothesis. *Science*, *317*(5843), 1360–1366. Retrieved from https://doi.org/10.1126%2Fscience.1146282 doi: 10.1126/science.1146282

Imura, T., & Tomonaga, M. (2013, nov). Differences between chimpanzees and humans in visual temporal integration. *Scientific Reports*, *3*(1). Retrieved from https://doi.org/10.1038%2Fsrep03256 doi: 10.1038/srep03256

Inoue, S., & Matsuzawa, T. (2007, dec). Working memory of numerals in chimpanzees. *Current Biology*, *17*(23), R1004–R1005. Retrieved from https://doi.org/10.1016%2Fj.cub.2007.10.027 doi: 10.1016/j.cub.2007.10.027

Kawai, N., & Matsuzawa, T. (2000, jan). Numerical memory span in a chimpanzee. *Nature*, *403*(6765), 39–40. Retrieved from https://doi.org/10.1038%2F47405 doi: 10.1038/47405

Kuramoto, Y. (2005). Self-entrainment of a population of coupled non-linear oscillators. In *International symposium on mathematical problems in theoretical physics* (pp. 420–422). Springer-Verlag. Retrieved from https://doi.org/10.1007%2Fbfb0013365 doi: 10.1007/bfb0013365

Lisman, J. E., & Jensen, O. (2013, mar). The theta-gamma neural code. *Neuron*, *77*(6), 1002–1016. Retrieved from https://doi.org/10.1016%2Fj.neuron.2013.03.007 doi: 10.1016/j.neuron.2013.03.007

Lisman, J. E., & Otmakhova, N. A. (2001). Storage, recall, and novelty detection of sequences by the hippocampus: Elaborating on the SOCRATIC model to account for normal and aberrant effects of dopamine. *Hippocampus*, *11*(5), 551–568. Retrieved from https://doi.org/10.1002%2Fhipo.1071 doi: 10.1002/hipo.1071

Lodi, M., Rossa, F. D., Sorrentino, F., & Storace, M. (2020, oct). Analyzing synchronized clusters in neuron networks. *Scientific Reports*, *10*(1). Retrieved from https://doi.org/10.1038%2Fs41598-020-73269-9 doi: 10.1038/s41598-020-73269-9

Loebel, A., & Tsodyks, M. (2002). Computation by ensemble synchronization in recurrent networks with synaptic depression. *Journal of Computational Neuroscience*, *13*(2), 111–124. Retrieved from https://doi.org/10.1023%2Fa%3A1020110223441 doi: 10.1023/a:1020110223441

Marchetti, G. (2014, aug). Attention and working memory: two basic mechanisms for constructing temporal experiences. *Frontiers in Psychology*, *5*. Retrieved from https://doi.org/10.3389%2Ffpsyg.2014.00880 doi: 10.3389/fpsyg.2014.00880

OpenAI. (2021). *GPT-3 API [API].* Retrieved from https://beta.openai.com/docs/api-reference/introduction

Panaggio, M. J., Ciocanel, M.-V., Lazarus, L., Topaz, C. M., & Xu, B. (2019, oct). Model reconstruction from temporal data for coupled oscillator networks. *Chaos: An Interdisciplinary Journal of Nonlinear Science*, *29*(10), 103116. Retrieved from https://doi.org/10.1063%2F1.5120784 doi: 10.1063/1.5120784

Persuh, M., LaRock, E., & Berger, J. (2018, mar). Working memory and consciousness: The current state of play. *Frontiers in Human Neuroscience*, *12*. Retrieved from https://doi.org/10.3389%2Ffnhum.2018.00078 doi: 10.3389/fnhum.2018.00078

Premack, D. (2007, aug). Human and animal cognition: Continuity and discontinuity. *Proceedings of the National Academy of Sciences*, *104*(35), 13861–13867. Retrieved from https://doi.org/10.1073%2Fpnas.0706147104 doi: 10.1073/pnas.0706147104

Read, D. W., Manrique, H. M., & Walker, M. J. (2022, mar). On the working memory of humans and great apes: Strikingly similar or remarkably different? *Neuroscience & Biobehavioral Reviews*, *134*, 104496. Retrieved from https://doi.org/10.1016%2Fj.neubiorev.2021.12.019 doi: 10.1016/j.neubiorev.2021.12.019

Shandilya, S. G., & Timme, M. (2011, jan). Inferring network topology from complex dynamics. *New Journal of Physics*, *13*(1), 013004. Retrieved from https://doi.org/10.1088%2F1367-2630%2F13%2F1%2F013004 doi: 10.1088/1367-2630/13/1/013004

Singer, W. (2009). Neural synchrony and feature binding. In *Encyclopedia of neuroscience* (pp. 253–259). Elsevier. Retrieved from https://doi.org/10.1016%2Fb978-008045046-9.00226-6 doi: 10.1016/b978-008045046-9.00226-6

Völter, C. J., Mundry, R., Call, J., & Seed, A. M. (2019, jul). Chimpanzees flexibly update working memory contents and show susceptibility to distraction in the self-ordered search task. *Proceedings of the Royal Society B: Biological Sciences*, *286*(1907), 20190715. Retrieved from https://doi.org/10.1098%2Frspb.2019.0715 doi: 10.1098/rspb.2019.0715

WikimediaFoundation. (2022). *Spatial memory - wikipedia.* Retrieved 2022-09-08, from https://en.wikipedia.org/wiki/Spatial_memory